Iris Kristin Koa

Calibration and development of a numerical method for frost protection

June 2019

NTNU
Norwegian University of
Science and Technology

NTNU

Norwegian University of
Science and Technology

Calibration and development of a numerical method for frost protection

Iris Kristin Koa

PREFACE

This paper is a master thesis written during the Spring semester of 2019 and constitutes the final work of the Master of Science program Civil and Environmental Engineering at the Norwegian University of Science and Technology (NTNU). The thesis is written within the master specialization Highway Engineering at the Department of Civil and Environmental Engineering (DCEE) and is a collaboration with the Norwegian Public Roads Administration (NPRA).

Trondheim, June 11, 2019
Iris Kristin Koa

Table of contents

Calibration and development of a numerical method for frost protection

Iris Kristin Koa[1]

ABSTRACT

Frost heave and spring thaw can be critical contributors to pavement deterioration in seasonal frost regions. Several numerical programs are available to predict frost penetration depth, but the lack of fixed material parameters often leads to unreliable estimates and hence inaccurate frost design. To prevent detrimental frost heave and spring thaw conditions in the foundation layers, adapting numerical models to site-specific conditions is essential. This study uses the module Heat transfer in porous media in COMSOL Multiphysics to model heat flux in seven full-scale road sections with different frost protective layers. Numerical models are built for each section, using actual ambient air temperature as the top boundary condition, and material properties are adjusted to fit temperature profiles measured over seven weeks. The models fit field data with an average accuracy of 0.56 °C. The final thermal properties for each material in the road structure are presented for use in further calibration. It is assumed that applying continuous surface measurements as the top boundary condition would be a key improvement for future work. A further recommendation is to increase the modeling period, preferably to a whole year consisting of a cold winter.

Keywords: Pavement design, frost protection materials, thermal properties, numerical analysis

1   INTRODUCTION

Frost heave and spring thaw can be critical contributors to pavement deterioration in the cold regions of the world like Northern Europe, large parts of Asia, Canada, Alaska, and about a third of the USA (1) (2). During winter time, uneven frost heave can reduce the functional performance of the structure, while during spring, water from thawing ice can lessen the bearing capacity and provide substantial unevenness (1). This can lead to costly repairs and reduction in the roads service life, as well as a poor ride quality for road users (3). The problem occurs when frost reaches frost susceptible ground causing volume expansion when freezing and an excess of water when melting. An essential aspect of the pavement design is therefore to predict actual frost depth and hinder the frost in reaching frost susceptible ground.

How deep the frost penetrates is mainly affected by climatic conditions, soil water content, layer thickness, and the materials thermal properties (4). Several numerical and analytical techniques are available to calculate heat transfer and estimate frost depth penetration (5). Still, the reliability of the methods varies, and the needed input data are often unavailable or expensive to collect, resulting in inaccurate outcomes (4). Some researchers have compared modeling results with field measurements to increase the accuracy (2) (4) (6). However, limited research has been done to calibrate the models and determine fixed thermal-physic parameters of road and soil materials.

Frost related problems have been an issue since the first constructed roads. Some of the earliest research on the topic was done in 1914 by Johanson (Sweden) and by Taber and Casagrande (USA) in the 1930s (7). The last extensive Norwegian work on frost penetration was done under a project called Frost I Jord during the years of 1970-76 (8). Since that, limited science has been carried out in Norway (8), despite the need for increased knowledge. From 2009 to 2011 in the south-eastern part of Norway, frost-related damage was reported on several newly built roads. This drew the public's attention and

---

[1] This master thesis (paper) was authored by Iris Kristin Koa with Inge Hoff and Jostein Aksnes as advisors, potential future submissions of this paper will be with Iris Kristin Koa, Inge Hoff and Jostein Aksnes as authors.

resulted in an investigation on the damaged roads performed by an expert group from the Norwegian Directorate of Public Roads (NDPR). The objective of the investigation was to suggest improvements for future frost protection in road superstructures (9).

Subsequently, two larger projects were carried out to build more knowledge on the topic. Between 2011 and 2017, the Norwegian Public Roads Administration (NPRA) performed several types of research and development projects called Varige Veger (10). Furthermore, from 2015 to 2019, a project called Frost Protection of Roads and Railways were investigated by the Norwegian University of Science and Technology (NTNU). Collaborators in the project are SINTEF Building and Infrastructure and University Laval in Canada (11). One of the main objectives in both projects was to improve the guidelines for frost protection of roads (and railways) (10) (12). During the same period, the handbook of guidelines for road structures in Norway (Handbook N200) was revised first in 2014 and again in 2018. However, the guidelines regarding frost design are founded on theory and communication with the building industry, and still need more investigation and scientific background (Jostein Aksnes, personal communication, 2018).

In 2018, the NPRA established a new research and development project called Analytical design of pavement structures. NPRA cooperates with NTNU, Swedish Transport Administration and Swedish National Road and Transport Research Institute, and the final product of the project will be a more advanced design system for pavement structures. One of the main objectives in the process is to establish field tests to calibrate design systems as well as adapting parameters to Norwegian conditions (Brynhild Snilsberg, personal communication). A field test with seven sections consisting of different frost protection layers was built in 2018 at Jaktøyen in Trondheim. Temperature sensors were installed in various depths to enable analysis of the material's thermal response and performance. This study attempts to reproduce the first available temperature data from Jaktøyen field test by building numerical models and adjusting material properties to fit the measurements. The following questions will be addressed:

- To what extent are numerical models useful for temperature modeling at Jaktøyen field test?
- Is it possible to generate a model that corresponds to measurements from all the seven sections?
- To what degree is it possible to obtain any fixed material parameters for further modeling?

2 HEAT TRANSFER ESTIMATION

The thermal system is complex, and it is challenging to calculate temperatures in pavements and estimate frost depth. Firstly, it is challenging to collect meteorological data regarding surface temperature (13). Air temperature, wind, precipitation, snow cover, solar radiation and radiation from heat exchange with clouds and gas layers in the atmosphere, can all influence on the heat transfer (5) (14). Secondly, varying stratification in the soil, as well as variations in the material's thermal properties, leads to complicated heat flow (13). Thirdly, all the thermal properties change with the water content, which is fluctuating with time (15).

According to the principle of conservation of energy, the heat flow out of the pavement must at any time equal the heat flow into the pavement plus the change in storage of heat (5). The heat balance can thus be used to predict pavement temperatures at any given time as well as temperature change over a more extended period. For soil materials with a frozen and unfrozen zone, the heat balance can be expressed as (5):

[1] $q_- = q_+ + q_f + q_s$ $[W/m^2]$

where q_- is the heat flow between the surface and the frost front through the frozen layer, q_+ the heat flow between the unfrozen soil and the frost front, q_f the latent heat from water to ice and q_s the heat

generated by the additional segregation of water during ice lens formation (5). q_- and q_+ are described by Fourier's law, where the conductive heat flux, q, is defined as proportional to the temperature gradient: $q = -k \cdot \nabla T$ (16).

Neumann suggested one of the first methods to calculate heat transfer in the 1860s. Stefan later modified the equation in 1891, where he solved Neumann's equation without considering the heat capacity (4). Stefan also assumed a homogenous layer of soil as well as a linear temperature profile. The equation can give an estimate of the frost index (FI) required to freeze the material to depth z (13):

[2] $$FI = f \cdot L \cdot \frac{z^2}{2 \cdot k}$$

where:
	FI	= Temperature · time [h°C] (frost index in hour degree Celsius)
	f	: conversion factor from MJ to Wh (1 MJ = 277,78 Wh)
	L	= ($L_w \cdot w_{vol}$) : volumetric latent heat of fusion [MJ/m^3]
	z	: frost penetration depth [m]
	k	: thermal conductivity [W/(m·K)]

Due to simplifications, the Stefan equation is shown to give relatively inaccurate results (2). Subsequently, several modifications are developed, among them the Watzingers method. As opposed to Stefan, Watzinger takes the heat capacity of soil into consideration. A note of Nordal gives the following description of the method, last revised in 2006 (13). Watzingers method assumes a pavement with the number of *n* frozen layers and *s ≥n+1* unfrozen layers beneath. The layers cool down from temperature T_H at the beginning of the frost period to T_V at the end of the same period. For the n first layers, the material starts to cool down from T_H to 0°C, then the latent heat releases and finally the material cools down to $-T_V$. The necessary frost index for this case is given in [*3*]. For the layers below the freezing front, where $T_V > 0$°C, only the necessary frost index to emit ground heat is calculated. Summing up the frost index for both cases gives the total amount of frost, see Eq. 3-5.

[3] $$FI = \sum_{i=1}^{n} Q_i (\sum_{j=0}^{i=1} R_j + \frac{R_i}{2})$$

[4] $$FI_{ground\ heat} = \sum_{i=n+1}^{s} Q_i (\sum_{j=0}^{i-1} R_j + \frac{R_i}{2})$$

[5] $$FI_{total} = FI + FI_{ground\ heat}$$

where:
	Q_i	= f·h$_i$· (C$_u$·T$_H$ + C$_f$·T$_V$ + L) for the frozen layers
	Q_i	= f·C$_u$· (T$_H$-T$_V$) ·h$_i$ for the layers below freezing front, both T$_H$ and T$_V$ > 0°C
	R	= h$_i$/ k
	h$_i$	: thickness of layer i [m]
	C$_u$, C$_f$	: heat capacity for unfrozen (u) and frozen (f) soil [MJ/(m^3·K)]
	All other factors like before.	

Table 1 shows two other modifications as well as Stefan equation expressed as frost depth z, included some assumptions and limitations.

Table 1 Frost depth equations with their respective assumptions and limitations

Equation	Name	Assumptions	Limitations	Reference
$$z = \frac{\sqrt{2 \cdot k \cdot FI}}{f \cdot L}$$	Stefan Equation	Neglect heat capacity; soil is uniform and isotropic; 1D; linear temperature profile	Overestimates frost depth due to no heat capacity	(13)

	Modified Berggren Equation	Homogenous ground; soil is uniform and isotropic; 1D	Ground is one dimensional; neglecting movement of water in freezing soil	(2)
$z = \lambda \dfrac{\sqrt{2 \cdot k \cdot FI}}{f \cdot L}$				
$z = 1{,}6968\sqrt{FI} - 12{,}91$	Chisholm and Phang	Software used to provide an accurate numerical solution on the Modified Berggren equation	Empirical equation based on local data	(4)

Later, numerical and analytical techniques have been used as a tool in frost design by modeling transient heat flow in pavement layers (5) (17) (18). Horvli et al. wrote in 2005 a review of four software programs for modeling, including the SSR model used at MTQ, Quebec, Canada, where frost penetration is based on the thermal balance at the frost front in homogeneous layers, and TEMP/W, based on the general heat flow equilibrium equation and used in several countries; including the USA, Canada, and Norway (5). Other similar software examples are ANSYS Workbench (USA), COMSOL Multiphysics (Sweden), Frost 3D Universal (Russia) and SV Office (Canada) (18). Modeling techniques have gained significant importance for pavement design (2), but the accuracy of the numerical models varies and is affected by available data (5) (6) (4) (19).

Comparing modeling results with field measurements can improve the accuracy of the numerical models. In 2006, two field test sites from the 1980s in Canada and Hamilton in the USA were used to compare frost penetration models with results from field measurements. The conclusion was that reliable models require correct values for the materials hydraulic and thermal properties as well as correct boundary conditions (5). In 2011, a similar study was performed in Korea where measured frost penetration depths along national roads were compared with results of empirical equations. This study developed a more accurate empirical equation adapted to local conditions, sun radiation, and snowfall (6). Next, several models were evaluated in 2015 with measurements from field test sites in Michigan and Minnesota. All showed disagreement between field measurements and model results, and in conclusion, correct values for the materials heat conductivity is essential for the results (19). Later, in 2018, a case study was performed in Iowa, USA, to compare field measurements with the modified Berggren and other simplified empirical models. By including site-specific information like geomaterial properties, foundation layer conditions, pavement type, and local climate, the accuracy of frost depth predictions will increase (2).

3 FIELD TEST AND THERMAL PROPERTIES

Location and pavement structure

The field test was constructed at Jaktøysletta as a part of a new four-lane E6 14 km south-southwest of Trondheim, in Trøndelag, Norway. The pavement was complete and open for traffic on the first of November 2018. AADT of the road is 13150 vh/day (20), and winter maintenance strategy is a bare road strategy with no acceptance for snow or ice on the surface, using a combination of ploughing and salting. The field test consists of seven sections, each with a length of 50 meters. All sections have a distinct frost protection layer designed according to the requirements in handbook N200 (2014 version) and should withstand a winter condition with 100 years return period.

Figure 1 shows cross-section for the seven field tests (F1-F7). The wearing course was not yet placed during this study (winter/spring 2019). All frost protection layers are well drained.
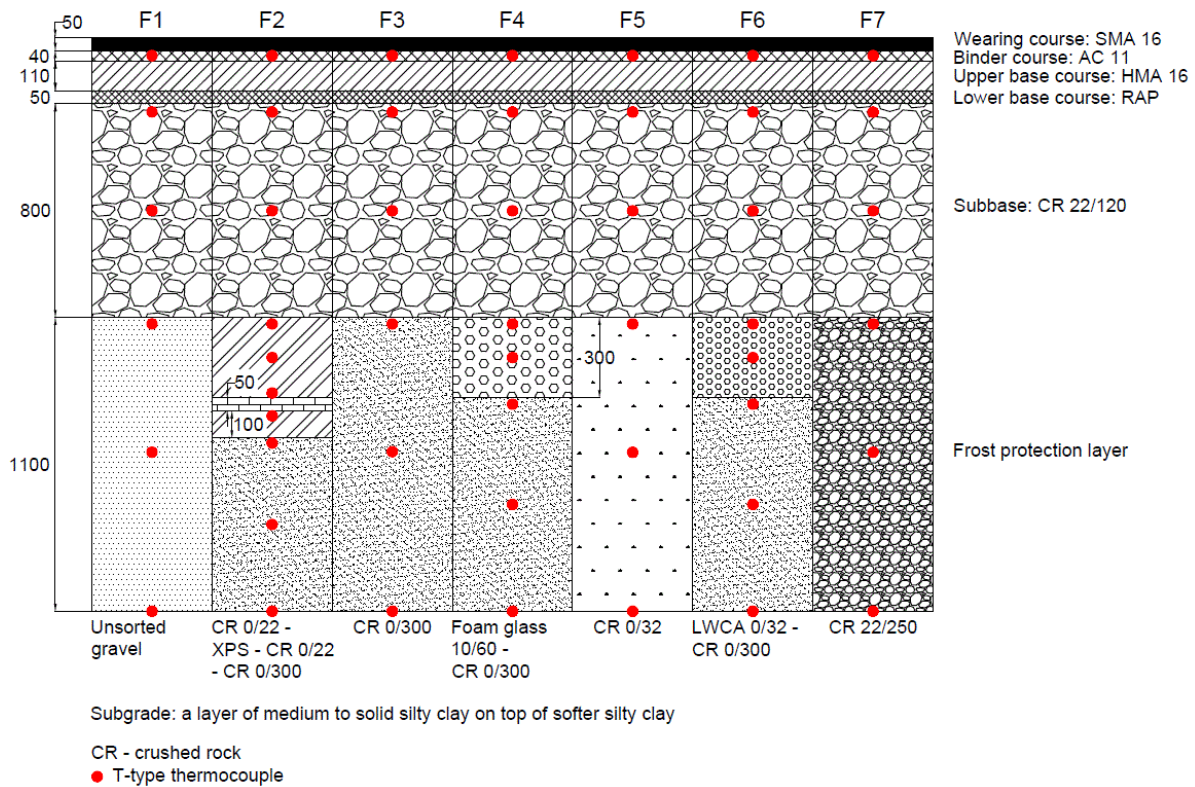
Figure 1 Cross-section of road segments (F1-F7) at Jaktøyen. Unit for depth: mm

In order to measure temperature distribution, each section is instrumented with T-type thermocouples. The sensors are either placed in the middle of a layer or 25 mm into the layer. Note that the sensors in the asphalt layer are embedded at the top of the binder course, which during the temperature logging was the topmost layer. In addition to the sensors marked on Figure 1, thermocouples are placed 250 mm and 475 mm into the subgrade for all sections, as well as sensors in the depth of 3.1 and 4.1 m in F1 and F7. Along with the thermocouples 250 mm into the subgrade, a sensor of the type thermistor is installed in each section. The thermistors compare with the rest of the sensors as they have higher accuracy. Finally, moisture sensors are placed in F1, F5, F6, and F7 at different depths, but measurements were not available for this winter.

Climatic conditions of location and field test weather

In this chapter, values for air temperature (T_a) are taken from yr.no at Skjetlein weather station (3.5 km north of the test site, 44 meters above sea level (MASL)) and precipitation measurements from Voll weather station (14 km north-east of the test site, 127 MASL). Jaktøyen is 19 MASL, the annual mean temperature is 5 °C (21), and the frost occurring statistically once every 100 years, FI_{100}, is 23798 h°C (22). Figure 2 shows air temperatures and precipitation from December 2018 to March 2019, included the frost season, the modeling period, and the days with measurements. Frost season is here defined as the period where the average daily air temperature is less than 0 °C, included all freezing/thawing periods at each end of this period if it results in net frost. Compared to FI_2 (5839 h°C) at Jaktøyen (21), the frost index for the winter of 2018-2019 (4351 h°C) is rather low.
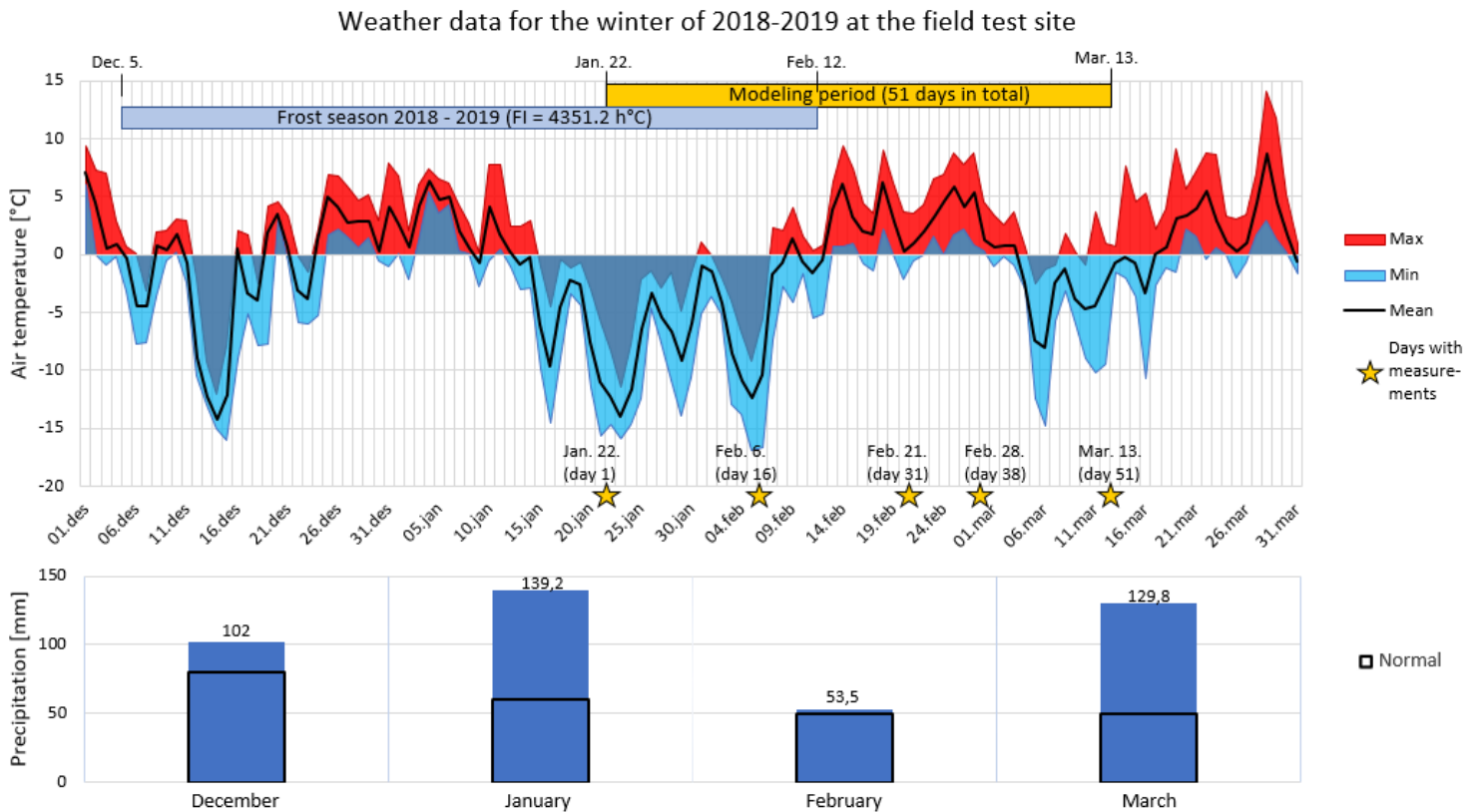
Figure 2 Weather data at Skjetlein weather station from December 2018 – March 2019

A dry November with mild weather may have resulted in relatively dry materials before the frost season started in December. Mainly rain was coming at the beginning of January, but later in the month, the precipitation came as snow. As a result of the bare road maintenance strategy, the snowfall has an insignificant impact on the heat transfer through the road surface but will reduce the heat loss at the side terrain. Precipitation in March came mainly as rain, which speeds up the melting process. Wind speed and solar radiation are not considered, but the new asphalt surface is dark and will absorb more heat than a light surface, resulting in more deviation between air and surface temperature.

Thermal conductivity

Thermal conductivity is the materials intrinsic ability to transfer heat. Rocks are polycrystalline aggregates, and the thermal conductivity is determined by the conductivity of each mineral forming the rock (23). Variations occur from around 2 W/mK for feldspar and mica to 3-5 W/mK for pyroxene and amphibole and 8 W/mK for quartz (23), leading to a range of variation in conductivity even within the same rock type (23). Furthermore, moisture content and porosity can affect the conductivity of rocks to a significant degree. For small amounts of water content (up to 10 %), there is an increase in thermal conductivity with increasing water content (23). For higher porosities, the contact between particles is decreasing and hence less effect from the particles on the conductivity. Further, micro-geometry (grading curve and particle shape) affects the porosity and is therefore also essential (7).

For lightweight clay aggregate (LWCA) and foam glass, thermal conductivity varies significantly with moisture content (14) because water and ice have considerable higher conductivity than air (7). A small variation also occurs for changes in temperature due to different conductivity for water and ice (24). Regarding extruded polystyrene (XPS), an insignificant amount of water is absorbed, and it retains its thermal properties for several years (25).

The specific conductivity of particles, k_s, is calculated for the rock and gravel material using:

[6] $$k_s = (k_n{}^{x_n}) = k_1{}^{x_1} \cdot k_2{}^{x_2} \cdot \ldots \quad [\frac{W}{mK}] \quad (26)$$

6

where x_n (n=1,2, …) is the volumetric decimal fraction of the content of minerals 1,2, … and k_n the thermal conductivity for component 1,2, … Share of minerals for the specific materials is taken from the Geological Survey of Norway, and values for thermal conductivity of each mineral is taken from Cermak and Rybach (1982) (23). Further, conductivity used in the numerical models is calculated for frozen (k_f) and unfrozen (k_{uf}) soil according to the generalized thermal conductivity model by Côté and Konrad (2004) (26). The calculated values were used as a guideline and hence adjusted in the numerical models during the calibration process.

Note: The six parameters marked in blue are the input values in the numerical model. Note that water content is included in all these parameters.

Specific heat and latent heat

The specific heat of a material at constant pressure, c_p, refers to the amount of heat per unit mass needed to raise the temperature by 1 K. For polycrystalline aggregates, the specific heat is given by the volumetric composition of the material and the specific heat of each component (7). Heat capacity varies with the porosity of the rock (if it is more than a few percent) and should be considered (27). Variations also occur for changes in temperature ($x \cdot 10^2$ °C) (27) but are not relevant for this study with variations from ± 20 °C.

Specific heat is calculated for the different rock material using:

[7] $$c_{p,s} = (x_n c_n) = x_1 c_1 + x_2 c_2 + \cdots \quad [\tfrac{J}{kgK}] \quad (27)$$

where $c_{p,s}$ is specific heat for particles, x_n (n=1,2, …) is the volumetric decimal fraction of the content of minerals 1,2, … and c_n (n=1,2, …) the specific heat per unit volume at constant pressure at a selected temperature, here 0 °C. Values for the specific heat of each mineral is taken from Cermak and Rybach (1982) (23) and Robertson (1988) (27). Finally, total specific heat for the composition of particles, fluid, and air is calculated for both frozen and unfrozen soil according to:

[8] $$c_{p,tot,f} = \frac{c_{p,s} \cdot \rho_s \cdot V_s + c_{p,i} \cdot \rho_i \cdot V_i}{\rho_{tot}} \quad [\tfrac{J}{kgK}]$$

[9] $$c_{p,tot,uf} = \frac{c_{p,s} \cdot \rho_s \cdot V_s + c_{p,w} \cdot \rho_w \cdot V_w}{\rho_{tot}} \quad [\tfrac{J}{kgK}]$$

where

[10] $$\rho_{tot} = V_s \cdot \rho_s + V_w \cdot \rho_w = \rho_d + V_w \cdot \rho_w \quad [\tfrac{kg}{m3}]$$

V_s is the volume of soil, ρ_d the dry density, $C_{p,w/i}$, $\rho_{w/i}$, and $V_{w/i}$ is specific heat, density, and volume of water/ice, respectively. All other factors are as before. As for the thermal conductivity, the calculated values from [8], [9] and [10] were used as a guideline and hence adjusted during the calibration.

Latent heat used in the numerical models is calculated according to

[11] $$L_{1-2} = \frac{L_w \cdot \rho_w \cdot V_w}{\rho_{tot}} \quad [\tfrac{kJ}{kg}]$$

where L_{1-2} is the latent heat between frozen (1) and unfrozen phase (2) and L_w is the latent heat of fusion (330 kJ/kg).

Road material parameters

Literature shows different values for material parameters in road construction, frequently based on empirical estimations. In the laboratory, it is possible to measure needed parameters, but in the design stage, this is often time-consuming and expensive, besides that the specific materials are often unknown at this stage. Table 2 shows a literature review with a range of parameter values for the

different layer materials. The values show significantly large variations, particularly for crushed rock (CR). The main reason for the variations in CR is probably different mineral content, grading curve, porosity, and water content for soil materials in earlier studies.

Table 2 Range of values for material parameters from the literature. k_f and k_{uf} are thermal conductivity for frozen and unfrozen ground, respectively, and $c_{p,f}$ and $c_{p,uf}$ are heat capacity for frozen and unfrozen ground, respectively. All other factors are as before.

Materials	ρ_d [kg/m³]	k_f [W/mK]	k_{uf} [W/mK]	$c_{p,f}$ [kJ/(m³K)]	$c_{p,uf}$ [kJ/(m³K)]
Asphalt	[2100, 2530]	[1.35, 1.5]	[1.35, 1.5]	[1190, 2520]	[1190, 2520]
Crushed rock	[1500, 2100]	[0.6, 1.9]	[0.4, 2.2]	[1330, 1830]	[680, 2019]
Foam glass	[125, 250]	[0.12, 0.15]	[0.04, 0.18]	[190, 313]	[190, 455]
LWCA	[280, 400]	[0.23, 0.24]	[0.12, 0.3]	578	952
XPS	[20, 100]	-	[0.023, 0.04]	-	1500
Subgrade (silt/clay)	[1200, 1800]	[1.6, 3.0]	[0.9, 1.8]	[1900, 2123]	[2700, 3200]

To reduce the number of variables in the calibration process, and because water content was assumed to be the most significant property for heat transfer, it was chosen to fix those properties independent of water content. Table 3 shows the set values for these properties for the different types of crushed rock and gravel at the test site. The values for *n* are assumed based on grain shapes and ordinary compaction in the field, where materials with more fines and variation in grain shapes are better packed and hence less porous.

Table 3 Fixed properties for the different materials in the superstructure, where ρ_s is specific density, n is porosity, and k_{dry} is dry thermal conductivity. All other factors are as before.

Materials	Supplier	Quarry/ gravel pit	ρ_s [kg/m³] *From supplier*	n [%] *Assumed*	ρ_d [kg/m³] $= \rho_s(1-n)$	k_s [W/mK] *Calculated in [6]*	$c_{p,s}$ [J/(kgK)] *Calculated in [7]*
CR 22/120	Franzefoss AS	Vassfjell	3040	0.41	1794	2.85	730
CR 0/22	Ramlo, dept. Sjøla	Sjøla	3040	0.30	2128	3.36	700
CR 0/32	Ramlo, dept. Sjøla	Sjøla	3040	0.32	2067	3.36	700
CR 22/250	Ramlo, dept. Sjøla	Sjøla	3040	0.45	1672	3.36	700
CR 0/300	Franzefoss AS	Vassfjell	3040	0.33	2037	2.85	730
Gravel 0/63	Søbstad AS	Furuhaugen	2700	0.27	1971	3.43	714
Foam glass	Glasopor AS	-	380	0.41	224	$k_{dry} = 0.097$	-
LWCA	Leca Norge AS	-	421	0.30	295	$k_{uf} < 0.12$	-
XPS	Brødr. Sunde AS	-	30	-	30	$k_{uf} = 0.033$	-

Water content for the subgrade was measured in the laboratory to a value of 18 % by weight. However, a time gap between excavation of the roadbed and the sampling led to some drying of the sample and the water content in situ is probably 10-20 % higher.

4   NUMERICAL MODEL

Model setup and calibration

A one-dimensional numerical solution of the temperature distribution was obtained using the finite element software COMSOL Multiphysics 5.4. A model with geometry and materials corresponding to the superstructure was created for all the seven sections. Initial- and boundary conditions were determined (see own paragraphs), and the output temperature profiles were compared to field measurements. Continuous temperature logging was not yet installed during the modeled period (2019-01-22/03-13), but five discrete measurements were available as shown in Figure 2. The heat transfer study was defined as a time-dependent transient analysis, where it by transient analysis means that temperature and heat flow vary with time. The time stepping method used was the backward Euler method with a strict time step of 1 day, and the models considered heat fluxes down to 4.13 m as the deepest (to the most profound temperature sensor). The accuracy of the thermocouples is 0.5 °C (28), hence, a temperature variance in ± 0.5 °C was considered as accurate results.

The models were calibrated by adjusting the six input material parameters: thermal conductivity (k_f, k_{uf}), heat capacity ($c_{p,tot,uf}$, $c_{p,tot,f}$), latent heat (L_{1-2}), and density (ρ_{tot}). The calibration was performed in two steps: first, changing the water content and hence all six water dependent input parameters, second, adjusting the conductivity and heat capacity independent of the water content to account for errors which might have been introduced by fixing the values in Table 3. Note that for each material property, the same value has been used in all seven models. Finally, a sensitivity analysis was performed by adjusting one parameter at the time.

Initial conditions

The temperature distribution from all sections registered at 22.01.2019 was treated as the initial conditions for the models. For all the layers in the superstructure, initial values were defined using average values between measurements from the top, middle, and bottom sensor of each layer. No measurements were available for the binder and base course; hence, the mean temperature for the surface and top subbase was used as initial temperature. For the subgrade, temperature gradients were used between depths with measured values.

Boundary conditions

The upper boundary condition was a time-varying function given by the daily mean air temperature distribution. As mentioned, measured surface temperatures were not available for the whole period, and air temperatures were therefore used. The bottom boundary condition was at first used at 5 m depth with the annual mean temperature for the test site location (5 °C (21)) as boundary value. Later, it was decided to instead use one of the most profound temperature sensors as a fixed bottom boundary with interpolated temperatures between the days with measurements.

Governing equations

The conduction of heat in an isotropic medium is given by the following differential equation (23):

[12] $$\frac{\partial T}{\partial t} = \kappa \Delta T + Q$$

where $\frac{\partial T}{\partial t}$ is the time derivative of the temperature, T the temperature field, Δ the Laplace operator, Q the heat source and κ is the thermal diffusivity (the rate at which heat is transferred in the soil) defined as the ratio of k, c_p and ρ_d of the soil mass according to:

[13] $$\kappa = \frac{k}{\rho_d c_p}$$

By inserting Eq. [13] in [12] the equation turns into a general time dependent heat equation, which is the principle for the heat transfer application module in COMSOL (16):

9

[14]
$$\rho c_p \frac{\partial T}{\partial t} = \nabla \cdot (k \nabla T) + Q$$

where the term $\nabla\cdot(k\nabla T)$ describes the conductive heat transfer in a solid. By including convective heat transfer in fluids, equation [14] turns into:

[15]
$$\rho c_p \frac{\partial T}{\partial t} + \rho c_p \boldsymbol{u} \cdot \nabla T = -\nabla \cdot \boldsymbol{q} + Q$$

where **u** is the velocity field and all other factors are as before. Finally, considered the effective thermal conductivity, k_{eff}, and effective volumetric heat capacity at constant pressure, $(\rho c_p)_{eff}$, the equation for heat transfer in porous media module in COMSOL is:

[16]
$$(\rho c_p)_{eff} \frac{\partial T}{\partial t} + \rho C_p \boldsymbol{u} \cdot \nabla T + \nabla \cdot \boldsymbol{q} = Q$$

where

[17]
$$\boldsymbol{q} = -k_{eff} \nabla T$$

Expressions for $(\rho C_p)_{eff}$ and k_{eff} is given in equation [18] and [21], respectively.

Phase change

The phase change from ice to water over constant temperature represents a discontinuous curve that is difficult to solve numerically. By introducing a small transition zone over which the temperature varies smoothly, the model is more amenable to numerical analysis (29). This is done by using an apparent heat capacity method. Defining the phase change temperature from ice (phase 1) to water (phase 2) as T_{1-2} and an interval of ΔT_{1-2} around the phase change, a transition function θ within this interval can represent a smooth transition between solid and liquid phase (30). The interval goes from $T_{1-2} - \frac{\Delta T_{1-2}}{2}$ to $T_{1-2} + \frac{\Delta T_{1-2}}{2}$, hence a state of mixed material properties finds place within ΔT_{1-2} (30). As the phase transition for water in road materials occurs at a very narrow temperature range, the transition interval was defined as 0.1 K. For the silty clay, a portion of unfrozen water will occur in sub-zero temperatures, and the transition interval for the subgrade was hence defined as 1 K.

o define heat capacity and thermal conductivity with respect to the phase change, two transition functions, θ_1 and θ_2, are used, see Figure 3. Effective values for thermal conductivity, specific heat, and density can then be defined at any time with respect to the transition functions. The following expression is used for effective heat capacity:

[18]
$$c_{p,eff} = \frac{1}{\rho_{eff}} \left(\theta_1 \rho_1 c_{p,1} + \theta_2 \rho_2 c_{p,2} \right) + L_{1-2} \frac{d\alpha_m}{dT}$$

where θ_1 and θ_2 is the fraction of frozen and unfrozen water (no units), $\rho_1 = \rho_2 = \rho_{tot}$ (assuming no expansion when freezing), $c_{p,1} = c_{p,tot, f}$ and $c_{p,2} = c_{p,tot,uf}$, L_{1-2} as before, α_m is the mass fraction given by

[19]
$$\alpha_m = \frac{1}{2} \frac{\theta_2 \rho_2 - \theta_1 \rho_1}{\theta_1 \rho_1 + \theta_2 \rho_2}$$

where the effective density is

Figure 3 Phase transition functions θ1 and θ2

[20]
$$\rho_{eff} = \theta_1 \rho_1 + \theta_2 \rho_2$$

The thermal conductivity with respect to the phase change is expressed as follows:

[21]
$$k_{eff} = \theta_1 k_1 + \theta_2 k_2$$

where $k_1 = k_f$ and $k_2 = k_{uf}$.

5   RESULTS

Figure 4 shows temperature distribution after adjusting the parameters as described in Model setup and calibration for day 16 and 51 together with registered temperatures.
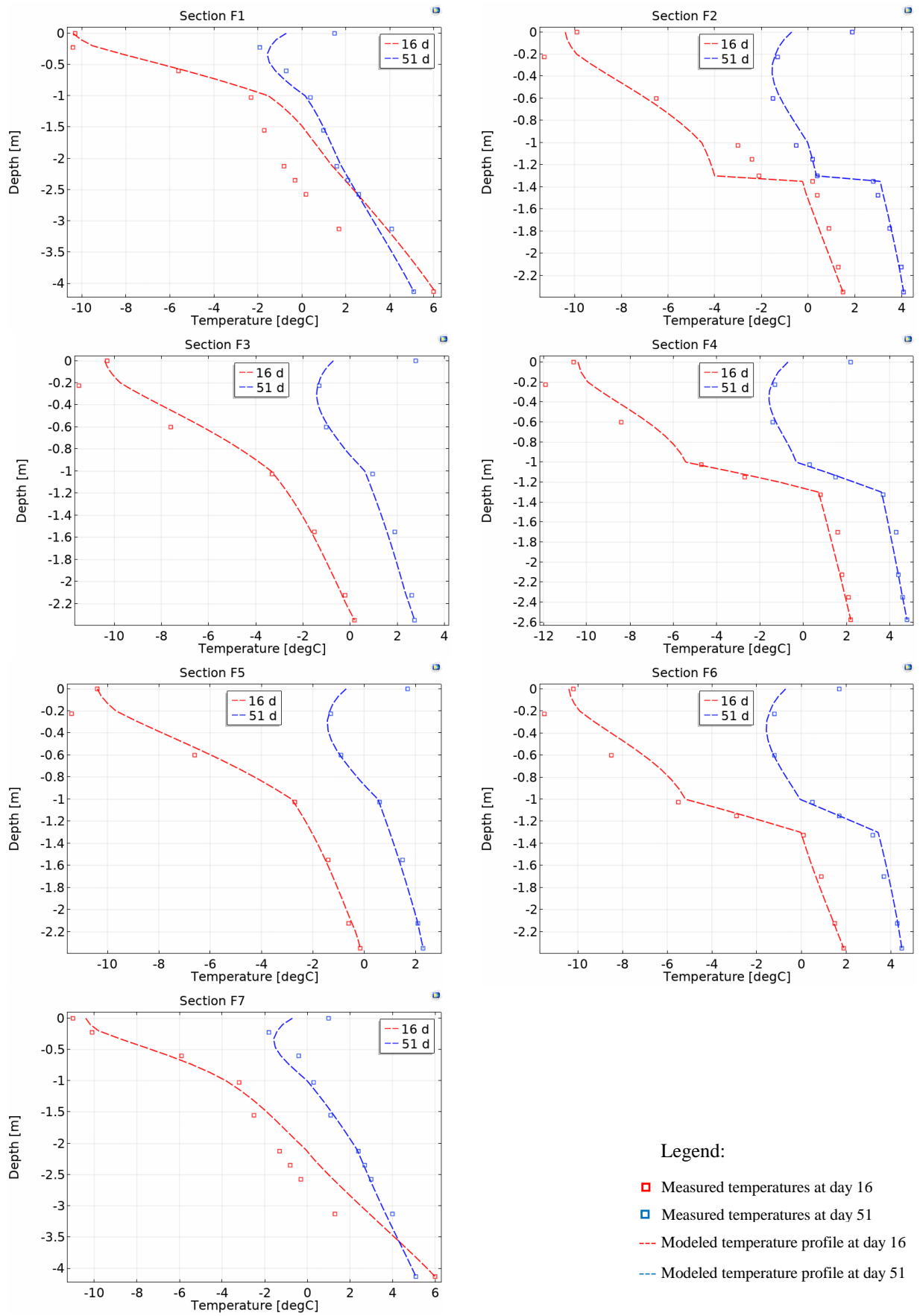
Figure 4 Temperature distribution from field measurements and numerical analysis

The deviation of modeled and measured temperature is presented by plotting the average of the deviations on day 16 and day 52 (average ΔT), see Figure 5 and Figure 6.
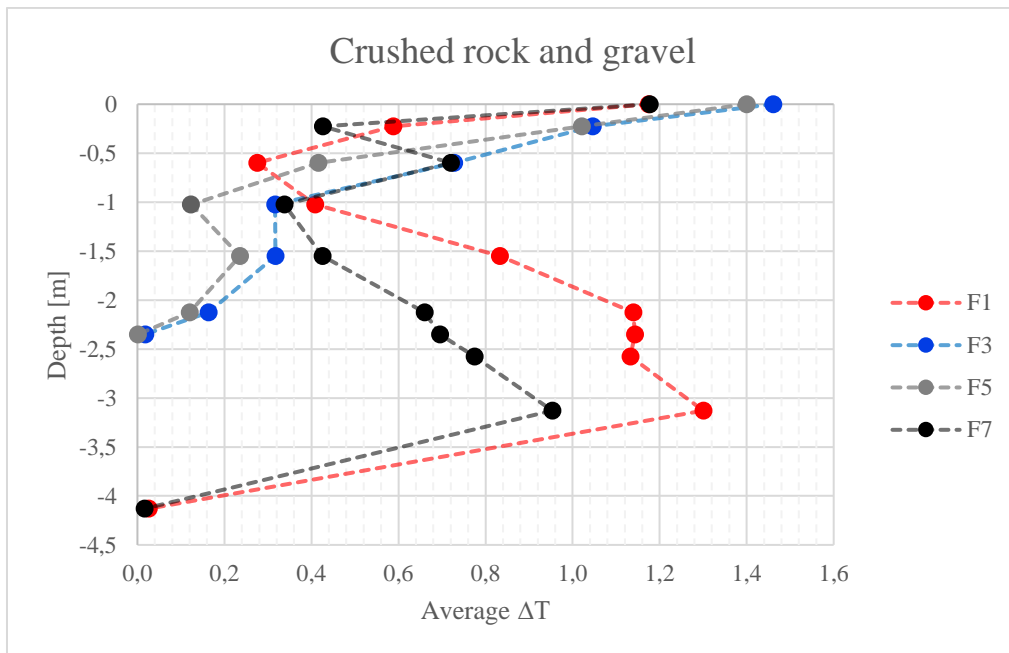
Figure 5 The average deviation of modeled and measured temperature per depth for the sections with CR and gravel as frost protection
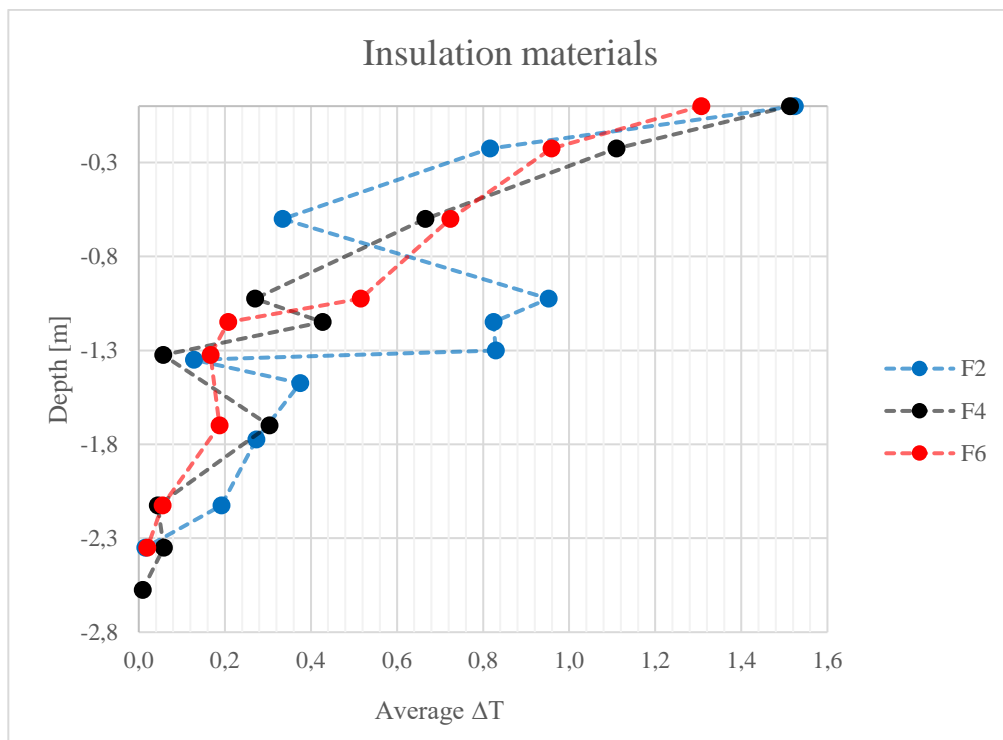
Figure 6 The average deviation of modeled and measured temperature per depth for the sections with insulation materials as frost protection

Mean deviation of all sensor depths is 0.80, 0.57, 0.58, 0.45, 0.47, 0.46 and 0.62 °C for F1, F2, F3, F4, F5, F6 and F7, respectively. Hence, F4-6 differ less than 0.5 °C from measurements, followed by F2, F3, and F7 with deviation around 0.6 °C and finally F1 with 0.8 °C. The total average deviation for the sections is 0.56 °C.

Table 4 shows the final material parameters used to get the presented results above. The given heat capacity is the product of $c_{p,tot}$ and ρ_{tot} used in the model.

Table 4 Final material properties used to get the presented results. Dry density (ρ_d) is unchanged from Table 3.

Layer	Materials	ρ_d [kg/m^3]	Water content [weight%]	k_f [W/mK]	k_{uf} [W/mK]	$C_{p,f}$ [kJ/(m^{3}K)]	$C_{p,uf}$ [kJ/(m^{3}K)]
Wearing/ binder/ base	Asphalt	2400	0	1.8 [1.25, 4.0]		1840 [72, 6000]	
Subbase	CR 22/120	1794	0.5	1.18 [0.9, 1.45]	1.0 [0.78, 1.35]	1337 [544, 1631]	1345 [725, 2630]
Frost protect-ion layer	CR 0/22	2128	1.5	2.1	2.0	1555	1624
	CR 0/32	2067	1.5	2.5 [1.9, 3.3]	2.4 [2.1, 3.1]	1510 [315, 2413]	1578 [630, 2518]
	CR 22/250	1672	0.5	1.3 [0.9, 1.7]	1.2 [0.8, 2.3]	1180 [168, 1680]	1200 [336, 1932]
	CR 0/300	2037	1	1.8 [1.3, 2.5]	1.7 [1.2, 2.3]	1518 [411, 3188]	1561 [1131, 3045]
	Gravel 0/63	1971	1.5	2.4 [1.4, 3.5]	2.2 [1.2, 3.4]	1467 [20, 5203]	1531 [20, 5203]
	Foam glass	224	1	0.11 [0.09, 0.16]	0.14 [0.10, 0.21]	193	198
	LWCA	295	1	0.16 [0.10, 0.22]	0.19 [0.10, 0.33]	275	281
	XPS	30	0	0.038 [0.029, 0.047]		45	
Subgrade	Silty clay	1425	33	3.3	1.8 [1.4, 2.25]	2071	3087 [1700, 4360]

According to the table, thermal conductivity is more decisive for heat transfer than the heat capacity, and the thermal conductivity for insulation materials is more sensitive for change than for crushed rock and gravel. Table 4 also shows the upper and lower value (in square brackets) for that parameter which changes the results 0.5 °C. Values for the asphalt, subbase, and subgrade, are tested in the model for section F3. The rest of the values are tested in the models containing the different materials. Models for section F5 and F7, where the frost reaches the subgrade, were used to test phase 1 for the silty clay. However, the frozen layer was too thin to give any effect and hence not possible to obtain a range. Further, ranges are excluded for CR 0/22, which is used as a protective layer and leveling course, not for thermal purposes and had only insignificant influence on the results. Finally, heat capacity for foam glass and lightweight aggregates gave negligible effects and hence excluded.

6 DISCUSSION

Several numerical programs are available to estimate frost penetration depth, but the lack of fixed material parameters in the design stage often leads to unreliable estimates and hence inaccurate frost design. This study aimed to investigate to what extent numerical analysis could be used to reproduce temperature measurement data from all the seven full-scale road sections at Jaktøyen, and to what extent any fixed material parameters could be established to use in further modeling. A reliable model and more information about specific materials thermal properties will increase the accuracy of the frost design and hence reduce pavement damage due to frost heave and spring thaw.

In this study, COMSOL Multiphysics was used to build numerical models consisting of the materials' thermal conductivity, heat capacity, density, and latent heat. The material parameters were calibrated by comparing numerical results with field measurements, and the final values used in the models are presented for each material. The results show that all models fit within a maximum average deviation of 0.8 °C from the field data. Due to a fixed bottom boundary and a less accurate top boundary, the most significant difference occurs at the surface, and the correspondence increases with depth until 100 % agreement at the bottom. All sections except F1 and F7 have a deviation less than 0.4 °C from depth 1.4 m and deeper. For F1 and F7, the difference is around 0.4 - 1.3 °C from 1.5 to 3.13 m due to the properties in the subgrade (discussed further down).

Water content

Water content is included in all the material parameters used as model input, and during the calibration, it was verified that water content largely influences the heat transfer as earlier stated from the literature. Finding the water content in the different materials is therefore crucial. The highest value used for latent heat responds to 1.5 % water content, which implies that the water content at Jaktøyen field test is lower than assumed for similar materials (4 % water content for drained frost protection layer of sand/gravel/crushed rock) in Handbook N200 (31). Three factors indicate that lower water content for the modeling period seems natural. Firstly, the frost protection layers are well drained and secondly, the preceding month of November was dry. Thirdly, the asphalt layer has cross-fall towards a ditch with yard manhole and will reduce the amount of water entering the pavement.

Change in moisture with time and depth was not considered in this study. Future work should try to include this in the modeling and investigate ways to easier predict water content for different materials, weather conditions, and other site-specific conditions. Defining the groundwater level could be of interest, as well as including moisture sensor data.

Road material parameters

Most of the presented material properties agree with values from the literature, yet some of them depart and will be discussed here. Thermal conductivity for the frozen ground is slightly lower than values found in the literature for foam glass and LWCA, 8% and 30% lower, respectively. The difference is probably due to lower water content than assumed in earlier studies. Since water has higher conductivity than the materials, lower water content gives lower conductivity. Further, the heat capacity for LWCA and XPS is smaller than those from the literature, but this is irrelevant since the heat capacity was found to be insignificant for the insulation materials.

Regarding the crushed rocks, values found in the literature for k_f and k_{uf} are up to 1.9 and 2.2 W/mK, respectively. The modeled conductivities for CR 0/22, CR 0/32 and the gravel are up to 1 W/mK higher than 1.9 and 2.2, even with low water content. The range of conductivity for the materials shows that the conductivity could be less and still fit within the range without affecting the result of more than 0.5 °C. Yet, to make the model fit with measured temperatures in the way it is presented, thermal conductivity had to be set as given in Table 4. The higher conductivities could have two possible reasons. The first reason could be a higher water content than used in the literature, which already is discussed to be less likely. The second and more credible explanation is a lower porosity

than assumed. The mentioned materials with high conductivity are from either Sjøla or Furuhaugen, with a higher k_s than the materials from Vassfjell. Hence, it seems like the particle conductivity greatly affects the final conductivity. Consequently, the porosity seems to be less in the field than assumed in the models. The porosity of the material is considered in agreement with professionals but is not measured in the field. By looking at the grain size distribution curves, all three CR 0/32, CR 0/22 and the gravel are well-graded materials, which indicates that the materials can be well packed and hence have a lower porosity than first assumed.

Additional observation shows that the thermal conductivity for crushed rock differs from values calculated with the model by Côté and Konrad (2005). According to this model, thermal conductivity should be lower for the current water content found in the calibration. For a CR 0/32 with $k_s = 3.36$ W/mK, porosity 32 % and water content 1.5 %, the method gives $k_f = 0.84$ and $k_{uf} = 0.94$ (26). The presented values for the same material are $k_f = 2.5$ and $k_{uf} = 2.4$, hence 2.98 and 2.55 times higher than those from the conductivity model. By looking at the range of material parameters from Table 4, the conductivity cannot reach the calculated values without decreasing the accuracy of the result of more than 0.5 °C. If the values from the calibration can be trusted, it seems like the input parameters used in the model by Côté and Konrad are wrong, meaning that the assumed porosity is too high or that the water content is too low. From the earlier discussion, too high porosity seems to be the most convenient explanation. However, several combinations of values for the input parameters in the numerical model can give similar results. Hence, more calibration is needed to find more accurate and reliable material properties before a conclusion can be drawn.

Subgrade

The modeled subgrade temperature seems less sensitive to air temperature than the field measurements. Considering F1 and F7 with temperature sensors down to the depth of 4.13 m, the numerical results give a warmer day 16 and a colder day 31 and 38 than compared to measurements. The same trend occurred when using 5 °C at 5 m depth as the bottom boundary. All the models cooled faster than in the field and eventually stayed at 1-2 lower degrees at day 31, 38 and 51, but the shape of the temperature curve was the same as for the field measurements. A possible reason could be that the thermal diffusivity in the subgrade is higher than used in the models. Hence, the conductivity must be higher, and the density and/or the heat capacity must be lower. By increasing the conductivity in the subgrade to around 3.5 W/mK and decreasing the volumetric heat capacity to about 2200 kJ/m^{3}K, more heat conducts faster and gives a higher correspondence with field data (except from day 16 which gets even warmer). However, these values exceed the range from the literature. Another explanation could be that the surface temperature remarkably affects the temperature in the subgrade and that the inaccurate top boundary is the reason.

Temperature sensors

An unnormal trend is observed between the last and second last bottom sensor, both the initial day and day 16, in all sections except F4. For F1 and F7, the distance between the two sensors is 1 m, but for F2, F3, F5, and F6 the distance is only 22.5 cm, and the change in temperature between them is up to 5.1 °C. Hence, the temperature gradient is up to 23 °C/m. The reason for this quick increase in temperature is hard to pinpoint. Differences between projected and built depths of the sensors are assumed to be small due to the use of GPS in the road construction. Further, a swap of the two most profound sensors could not be the case since the temperature in the subgrade is increasing with depth and the most profound sensors show the highest temperature. Additionally, the accuracy of each thermocouple is as mentioned ± 0.5 °C and should not show that wrong temperatures. Hence, the second deepest sensor was used as the bottom boundary rather than the deepest to avoid these uncertain measurements.

Assumptions and limitations

The first limitation for the study is the winter of 2018-2019 which turned out to be milder than a FI_2-winter for the test site location, and hence less appropriate for calibration of frost protective materials. A second limitation is to only have five discrete temperature registrations at the end of the winter instead of continuous measurements during the whole winter (planned in the continuation of the project). Because of the lack of continuous measurements, the top boundary condition was based on air temperatures where variance up to 3 °C was observed between air temperature and the actual measured surface temperature. The dark asphalt absorbs more sun radiation and will contribute to higher difference. Also, more wind and rain are assumed to be present in a mild period, which might give higher difference between temperatures at the weather station (air temp.) and the field test location (surface temp.). These sources of errors made unreliable results in the mild period, and day 31 and 38 were disregarded in the calibration process. As mentioned, the results still show a trend in higher deviation closer to the surface, but for the frost period, the results were expected to be decent. The fact that the top boundary differs from real conditions lowers the ability to generalize the findings. However, as the most significant deviation occurs at the surface and decreases with depth, models in future work with surface measurements as top boundary condition could give considerably improved results.

The rest of the assumptions regarding boundary conditions seems reliable. Snow maintenance was performed according to a bare road strategy and considering the accumulation of ice and snow on the road surface was therefore irrelevant. Regarding the bottom boundary, the use of measured temperatures makes the calibration more reliable. For the boundary facing the terrain side, the cross-section of the road shows that the ditch continues into a noise barrier and masses lie against the pavement at all points. Besides, snow has an insulation effect on the side terrain during wintertime. Hence it appears reliable to assume a zero-heat-flux at the edge. For future work, it seems favorable to measure temperatures also at the edge of the road to quantify any transversal temperature gradients. Early in this study, a two-dimensional model including edge effects, was set up and compared to the 1D model. This suggested that the results from both 1D and 2D were similar. For the last boundary, facing three further traffic lanes, it seems reliable to neglect a horizontal heat transfer between the lanes. Accordingly, a one-dimensional model was assumed to be the most convenient for this study.

Further assumptions are made to estimate frost depth without an excessively complicated model, and only features that are assumed to affect the results significantly are considered. It is assumed that the soil layers are isotropic and homogenous and that the pressure in the pavement is constant. Information about the real soil condition over time is not available, but the effect is probably insignificant and by disregarding these conditions, the model gets simpler and hence more reliable in this case. By the same argument, the influence of radiation is not considered. It is also assumed a negligible effect of natural air convection in the pavement, which for all sections except F7 seems reasonable. For F7 containing frost protection layer with an open graded material, air convection could be promoted due to relatively high intrinsic permeability and could be considered in future work.

7   CONCLUSION AND RECOMMENDATION

Accurate material parameters will decrease some of the uncertainties associated with frost depth prediction. Limited research has been done in order to decide fixed parameters by comparing numerical results with field measurements. This study has shown that numerical models are able to reproduce measured temperature profiles from all the seven sections at Jaktøyen field test with an average accuracy of 0.56 °C, and suggests thermal properties for all relevant materials. Limitations in the currently available measurements from this ongoing field test, both in frequency and duration, calls for further adjustment when more data has been generated. However, the method is found useful, and the parameters have been adapted to local conditions, which will facilitate further calibrations to finally obtain generalized parameters for the NPRA's future pavement design system.

It is recommended that further work continue to calibrate numerical models by including site-specific information and field measurements. It is assumed that applying continuous surface measurements as the top boundary condition would be a key improvement. A further recommendation is to increase the modeling period, preferably to a whole year consisting of a colder winter than the relatively mild one used in this study. Methods to better predict water content in road materials should also be investigated. Finally, further work could benefit from using mathematical tools to estimate optimal material parameters from field data, such as the inverse modeling method "Parameter estimation study" in COMSOL Multiphysics.

8   ACKNOWLEDGEMENTS

9   REFERENCES

1. **Simonsen, E., Isacsson, U.** *Thaw weakening of pavement structures in cold regions.* Stockholm, Sweeden : Cold Regions Science and Technology 29 (1999) 135–151, 1999.

2. **Zhang, Y., et al.** *Seasonal Frost Penetration in Pavements with Multiple Layers.* Iowa : American Society of Civil Engineers, 2018.

3. **Schaus, L. and Popik, M.** *Frost Heaves: A Problem That Continues To Swell.* Toronto, Canada : s.n., 2011.

4. **Rajaei, P. and Baladi, G. Y.** *Frost Depth - General Prediction Model.* s.l. : Department of Civil and Environmental Engineering, Michigan State University, 2015.

5. **Horvli, I.; Øiseth, E.; Henry, K.** *A review and reliability assessment of frost penetration models.* 2005.

6. **Hong, S.S., et al.** *A study on the frost penetration depth using measured value from pavement in Korea.* 2011.

7. **Heiersted, Roy S, et al.** *Frost I Jord.* 17. Oslo : Vegdirektoratet/NTNF, 1976. (Norwegian).

8. **Rieksts, K., et al.** The presence of natural air convection in road structural layers: comparison between field observations and numerical model. *Heat Transfer Characteristics of Crushed Rock and Lightweight Aggregate Materials.* Trondheim : s.n., 2018.

9. **Norwegian Directorate of Public Roads.** *Telehiv på nye norske veger - hvorfor, og hva kan gjøres for å unngå dette?* s.l. : Statens vegvesens rapporter, 2012. (Norwegian).

10. **Bakløkk, L. J.** *Varige veger.* s.l. : Statens vegvesens rapporter, 2017. (Norwegian).

11. *FROST-prosjektet: Nye harde og kalde fakta.* **Kuznetsova, E. and Hoff, I.** 02, 2017, Våre veger. (Norwegian).

12. **Kuznetsova, E., Hoff, I. and Danielsen, S. W.** Frost Protection of Roads and Railways. 2016.

13. **Nordal, R. S.** *Frysedjup i vegkonstruksjonar.* s.l. : Institutt for veg- og jernbanebygging, Norges teknisk-naturvitenskapelige universitet, 1989. (Norwegian).

14. **Øiseth, E.; Aabøe, R.; Hoff, I.** *Field test comparing frost insulation materials in road construction.* Trondheim : SINTEF & Statens vegvesen, 2006.

15. **Berntsen, Geir.** Frost design/use of frost protection layer. [Online] 07 24, 2013. [Cited: 06 02, 2019.] https://www.ntnu.no/documents/11617880/37574468/10-BCRRA2013+WS+Frost-Berntsen-frost+protection+design.pdf/ef4049f6-dae8-4707-ac3c-2ee3a8bc83df.

16. **Huc, N.** COMSOL BLOG. *Conjugate Heat Transfer.* [Online] 01 06, 2014. [Cited: 03 05, 2019.] https://www.comsol.com/blogs/conjugate-heat-transfer/.

17. **Øiseth, E. and Refsdal, G.** *Lightweight Aggregates as Frost Insulation in Roads - Design Chart.* Trondheim, Oslo : SINTEF, SVV, 2006.

18. **Alekseev, A., Gribovskii, G. and Vinogradova, S.** *Comparison of analytical solution of the semi-infinite problem of soil freezing with numerical solutions in various simulation software.* s.l. : IOP Publishing Ltd., 2018.

19. **Rajaei, P. and Baladi, G. Y.** *Predictive modeling of freezing and thawing of frost-susceptible soils.* 2015.

20. **Norwegian Public Roads Administration.** Vegkart. [Online] 2018. [Cited: 03 05, 2019.] https://www.vegvesen.no/vegkart/vegkart. (Norwegian).

21. ,**Norwegian Public Roads Administration.** Frostsonekart. [Online] 2018. [Cited: 03 04, 2019.] http://www.vegvesen.no/kart/visning/frostsonekart. (Norwegian).

22. **Norwegian Public Roads Administration.** Årsmiddeltemperatur. [Online] 2018. [Cited: 04 09, 2019.] www.vegvesen.no/kart/visning/arsmiddeltemperatur. (Norwegian).

23. **Cermak, V., Rybach, L.** *Thermal properties: Thermal conductivity and specific heat of minerals and rocks.* 1982.

24. **Furuberg, T.** *Leca isolasjon i veg og bane - termiske analyser.* Trondheim : SINTEF, 1998. (Norwegian).

25. **Andersland, O. B. and Ladanyi, B.** *Frozen Ground Engineering Second.* New Jersey : Americal Society of Civil Engineers & John Wiley & Sons, Inc., 2004.

26. **Côté, J., Konrad, J.-M.** *A generalized thermal conductivity model for soils and construction materials.* Québec : s.n., 2004.

27. **Robertson, E. C.** *Thermal properties of rocks.* Reston, Virgina : United States Department of The Interior Geological Survey, 1988.

28. **REOTEMP Instrument Corporation.** Thermocouple Info. *Thermocouple Accuracies.* [Online] 2011. [Cited: 06 13, 2019.] https://www.thermocoupleinfo.com/thermocouple-accuracies.htm.

29. **Frei, W.** COMSOL BLOG. *Thermal Modeling of Phase-Change Materials with Hysteresis.* [Online] 03 24, 2016. [Cited: 03 05, 2019.] https://www.comsol.com/blogs/thermal-modeling-of-phase-change-materials-with-hysteresis/.

30. **Bannach, N.** COMSOL BLOG. *Phase Change: Cooling and Solidification of Metal.* [Online] 08 12, 2014. [Cited: 03 05, 2019.] https://www.comsol.com/blogs/phase-change-cooling-solidification-metal/.

31. **Norwegian Directorate of Public Roads.** *N200 Vegbygging.* s.l. : Statens vegvesen, 2018. (Norwegian).

10 APPENDIXES

Appendix 1 – Floor plan over field test sections at Jaktøyen
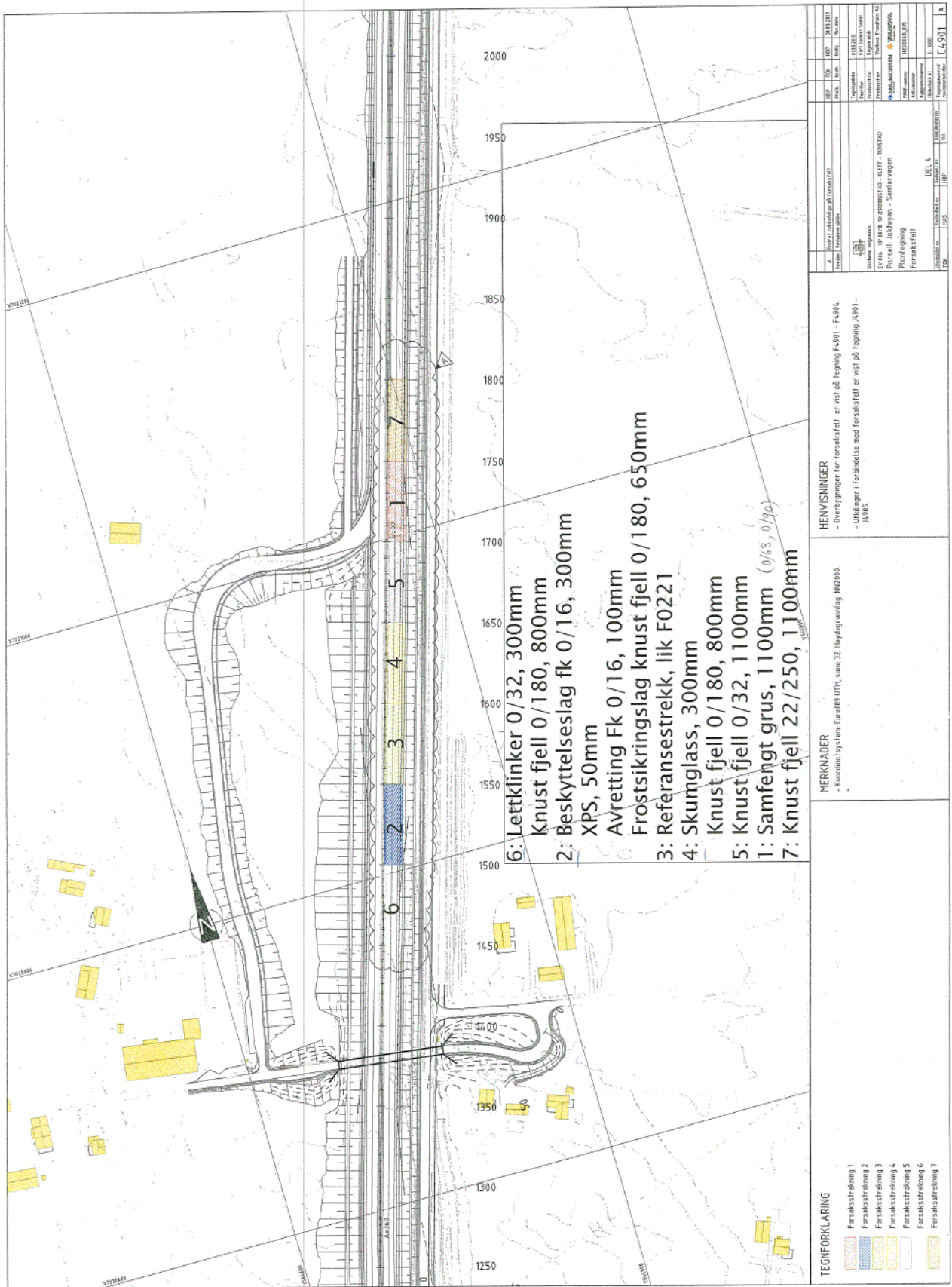
Figure 1 Floor plan over section F1-F7 at Jaktøyen

Appendix 2 – Road cross section of the field test
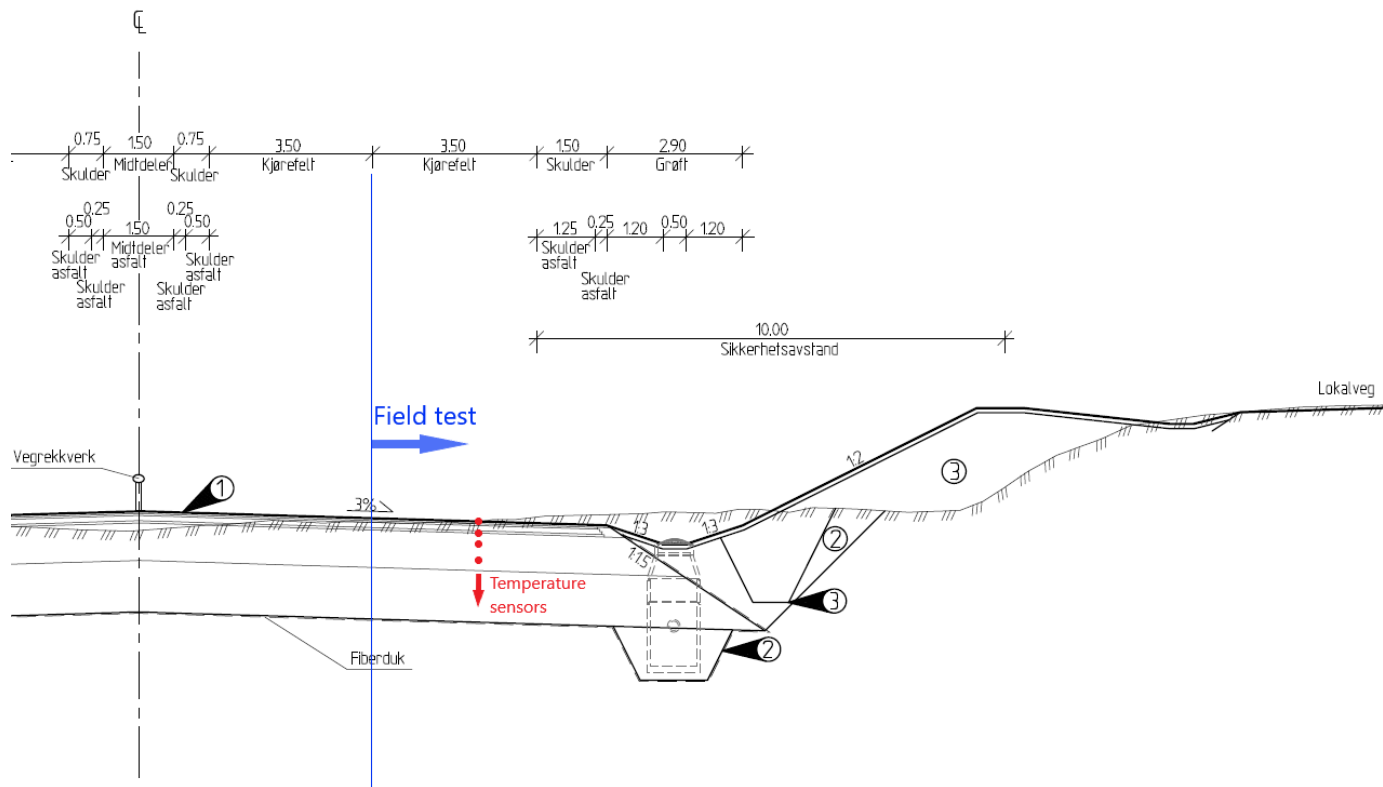
Figure 2 Part of cross section for E6 at Jaktøyen with the field test as the outer north going lane

Appendix 3 – Installed temperature sensors and moist sensors

Table 1 Installed thermocouples (black) and thermistor together with thermocouple (orange)

F1	F2	F3	F4	F5	F6	F7
Surface	Surface	Surface	Surface	Surface	Surface	Surface
22,5	22,5	22,5	22,5	22,5	22,5	22,5
60	60	60	60	60	60	60
102,5	102,5	102,5	102,5	102,5	102,5	102,5
	115		115		115	
	130		132,5		132,5	
	135					
155	147,5	155		155		155
	177,5		170		170	
212,5	212,5	212,5	212,5	212,5	212,5	212,5
235	235	235	235	235	235	235
257,5	257,5	257,5	257,5	257,5	257,5	257,5
313						313
413						413
[cm]	[cm]	[cm]	[cm]	[cm]	[cm]	[cm]

Table 2 Installed moist sensors

F1	F5	F6	F7
	128	155	
235		212	235
[cm]	[cm]	[cm]	[cm]

(22.01.2019)

F1 Sensor	Temp	F2 Sensor	kl 14:45 Temp	F3 Sensor	Temp	F4 Sensor	Temp	F5 Sensor	Temp	F6 Sensor	kl 13:20 Temp	F7 Sensor	Temp
8	-11	12	-14,9	8	-15,5	10	-14,1	8	x	10	-14,2	8	-13,6
7	-9,6	11	-11,7	7	-11,9	9	-11,6	7	-12,8	9	-11,7	7	-10,7
6	-3,5	10	-5,5	6	-5,8	8	-5,9	6	-6,3	8	-6,2	6	-4,5
5	-0,3	9	-3,2	5	-2,2	7	-2,6	5	-2,4	7	-2,9	5	-2,2
4	0,4	8	-2,5	4	-0,8	6	-1,2	4	-0,9	6	-1,6	4	-0,9
3	1,2	7	-2,3	3	0,0	5	1,4	3	-0,3	5	0,3	3	0,1
2	1,6	6	0	2	0,2	4	1,9	2	0	4	0,7	2	0,4
1	2,1	5	0,1	1	5,3	3	2	1	4,3	3	1,2	1	0,7
-1	3,5	4	0,5			2	2,1			2	1,4	-1	1,3
-2	6,6	3	0,9			1	2,3			1	6,3	-2	6,4
		2	1										
		1	5,8										

(06.02.2019)

F1 Sensor	Kl 14:15 Temp	F2 Sensor	kl 14:08 Temp	F3 Sensor	kl 14:02 Temp	F4 Sensor	kl 13:57 Temp	F5 Sensor	kl 13:46 Temp	F6 Sensor	kl 13:34 Temp	F7 Sensor	kl 13:25 Temp
10	-10,3	12	-9,9	8	-10,3	10	-10,6	8	x	10	-10,2	8	-11,0
9	-10,4	11	-11,3	7	-11,5	9	-11,9	7	-11,43	9	-11,5	7	-10,1
8	-5,6	10	-6,5	6	-7,6	8	-8,4	6	-6,64	8	-8,5	6	-5,9
7	-2,3	9	-3,0	5	-3,3	7	-4,7	5	-2,74	7	-5,5	5	-3,2
6	-1,7	8	-2,4	4	-1,5	6	-2,7	4	-1,43	6	-2,9	4	-2,5
5	-0,8	7	-2,1	3	-0,2	5	0,8	3	-0,60	5	0,1	3	-1,3
4	-0,3	6	0,2	2	0,2	4	1,6	2	-0,15	4	0,9	2	-0,8
3	0,2	5	0,4	1	4,0	3	1,8	1	3,27	3	1,5	1	-0,3
2	1,7	4	0,92			2	2,1			2	1,9	-1	1,3
1	6,1	3	1,32			1	2,2			1	5,7	-2	6,0
		2	1,5										
		1	5,3										

(21.02.2019)

F1 Sensor	Kl 11:22 Temp	F2 Sensor	kl 11:12 Temp	F3 Sensor	kl 11:26 Temp	F4 Sensor	kl 11:09 Temp	F5 Sensor	kl 11:05 Temp	F6 Sensor	kl 11:24 Temp	F7 Sensor	kl 11:02 Temp
10	1,7	12	1,3	8	1,5	10	1,1	8	x	10	1,5	8	1,8
9	1,7	11	2,1	7	1,4	9	1,5	7	1,5	9	1,5	7	1,4
8	1,4	10	1,4	6	1,2	8	1,2	6	1,2	8	1,1	6	1,0
7	0,9	9	0,3	5	0,7	7	0,6	5	0,7	7	0,7	5	0,6
6	1,4	8	0,9	4	1,6	6	0,8	4	1,5	6	1,1	4	0,7
5	2,1	7	1,0	3	2,5	5	3,5	3	2,2	5	3,0	3	1,9
4	2,6	6	3,2	2	2,8	4	4,2	2	2,5	4	3,6	2	2,3
3	3,1	5	3,4	1	3,2	3	4,4	1	2,7	3	4,2	1	2,7
2	4,5	4	3,9			2	4,7			2	4,5	-1	4,1
1	5,8	3	4,3			1	4,9			1	5,2	-2	5,6
		2	4,4										
		1	4,9										

Figure 3 Measured data from field (22.01, 06.02 and 21.02.2019). Sensor 1, 2, … are respectively the most profound sensor, second most profound etc.

(28.02.2019)

F1	Kl 10:48	F2	kl 10:47	F3	kl 10:48	F4	kl 10:48	F5	kl 10:48	F6	kl 10:47	F7	kl 10:48
Sensor	Temp	Sensor	Temp	Sensor	Temp	Sensor	Temp	Sensor	Temp	Sensor	Temp	Sensor	Temp
10	2,4	12	1,9	8	2,4	10	1,7	8	x	10	2,5	8	2,4
9	3,3	11	4,4	7	3,2	9	2,8	7	3,1	9	3,3	7	3,3
8	2,4	10	2,5	6	3,1	8	2,4	6	2,5	8	2,9	6	2,6
7	1,2	9	0,4	5	2,3	7	0,8	5	1,0	7	2,1	5	1,8
6	1,6	8	1,0	4	2,4	6	0,9	4	1,7	6	2,4	4	1,6
5	2,3	7	1,1	3	2,9	5	3,3	3	2,3	5	3,5	3	2,3
4	2,7	6	3,2	2	3,0	4	4,0	2	2,6	4	3,9	2	2,6
3	3,2	5	3,3	1	3,0	3	4,2	1	2,5	3	4,5	1	3,0
2	4,5	4	3,8			2	4,4			2	4,7	-1	4,1
1	5,5	3	4,2			1	4,5			1	5,0	-2	5,4
		2	4,3										
		1	4,7										

(13.03.2019)

F1	Kl 14:34	F2	Kl 14:34	F3	Kl 14:34	F4	Kl 14:34	F5	Kl 14:34	F6	Kl 14:34	F7	Kl 14:34
Sensor	Temp	Sensor	Temp	Sensor	Temp	Sensor	Temp	Sensor	Temp	Sensor	Temp	Sensor	Temp
10	1,5	12	1,9	8	2,08	10	2,2	8	x	10	1,7	8	1,0
9	-1,9	11	x	7	-1,32	9	-1,3	7	-1,3	9	-1,2	7	-1,8
8	-0,7	10	-1,5	6	-1,04	8	-1,4	6	-0,9	8	-1,2	6	-0,4
7	0,4	9	-0,5	5	0,97	7	0,3	5	0,6	7	0,5	0	0,3
6	1,0	8	0,2	4	1,91	6	1,5	4	1,5	6	1,7	4	1,1
5	1,6	7	0,4	3	2,63	5	3,7	3	2,1	5	3,2	3	2,4
4	2,1	6	2,8	2	2,75	4	4,3	2	2,3	4	3,7	2	-10,8
3	2,6	5	3,0	1	2,99	3	4,4	1	2,6	3	4,3	1	3,0
2	4,1	4	3,5			2	4,6			2	4,5	-1	4,0
1	5,1	3	4,0			1	4,8			1	4,8	-2	5,1
		2	4,1										
		1	4,3										

Figure 4 Measured data from field (28.02 and 13.03.2019). Sensor 1, 2, ... are respectively the most profound sensor, second most profound etc.

Appendix 5 – Calculations used for phase change materials

```
┌─────────────┐
│     AIR     │
├─────────────┤
│    WATER    │
├─────────────┤
│             │
│    SOIL     │
│             │
│             │
└─────────────┘
```
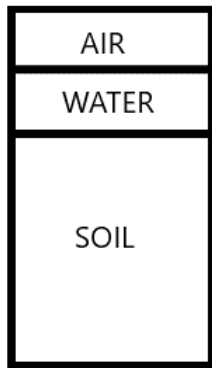
n - porosity

w – water content (% by weight)

$V_s = 1 - n$

$\rho_d = \rho_s \cdot V_s$

$V_w = w \cdot (\rho_d/\rho_w)$

Assumes no expansion when freezing → $V_w = V_{ice}$ and $\rho_w = \rho_i$

$L_w = 330$ kJ/kg

$$\rho_{tot} = V_s \cdot \rho_s + V_w \cdot \rho_w \quad [\text{kg/m}^3]$$

$$C_{p,tot,uf} = \frac{C_{p,s} \cdot \rho_s \cdot V_s + C_{p,w} \cdot \rho_w \cdot V_w}{\rho_{tot}} \quad [\text{J/kgK}]$$

$$C_{p,tot,f} = \frac{C_{p,s} \cdot \rho_s \cdot V_s + C_{p,i} \cdot \rho_i \cdot V_i}{\rho_{tot}} \quad [\text{J/kgK}]$$

$$L = \frac{L_w \cdot \rho_w \cdot V_w}{\rho_{tot}} \quad [\text{kJ/kg}]$$

Appendix 6 – Calculation of the frost index (FI)
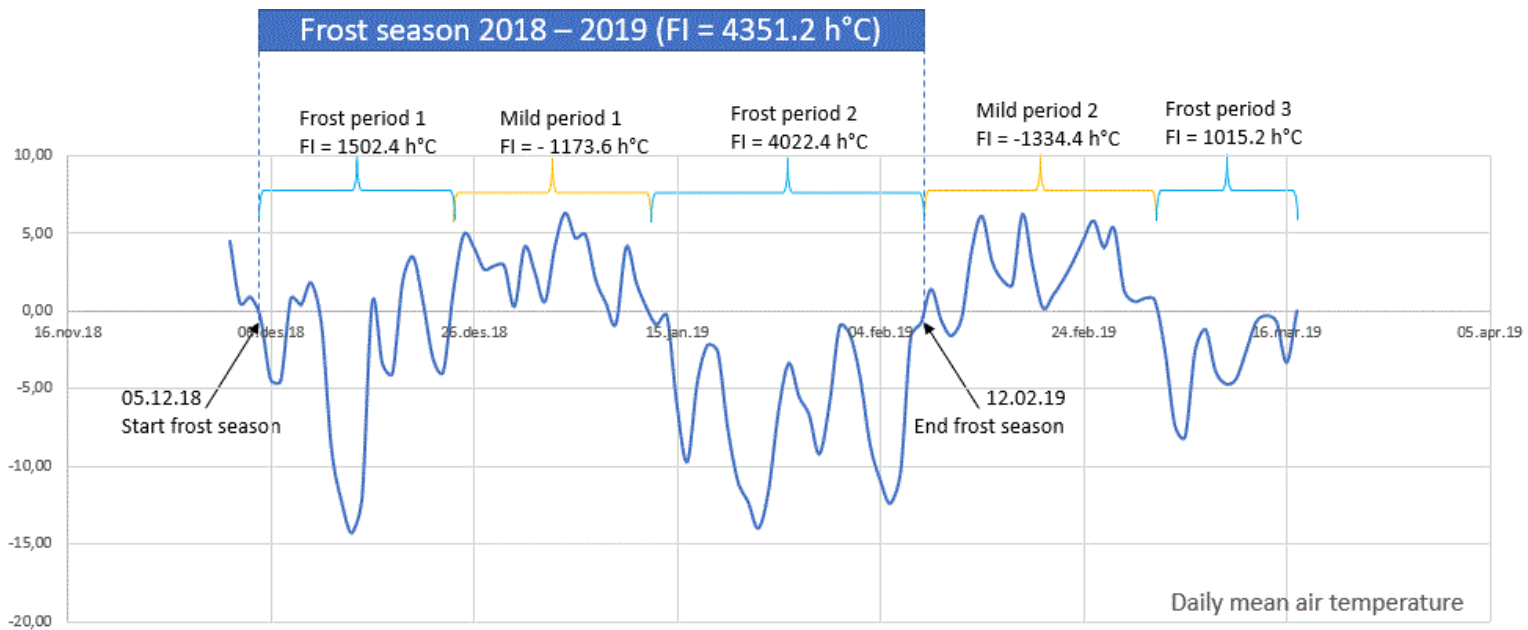
Figure 5 The frost season 2018 - 2019

Frost season is defined as the period where the average daily air temperature is less than 0 °C, included all freezing/thawing periods at each end of this period if it results in net frost (Norwegian Standard, NPRA/NDPR, 2019).

We have that:

| FI (frost period 1) | > | FI (mild period 1) | → Results in net frost → Start frost season 05.12.18

| FI (frost period 3) | < | FI (mild period 2) | → Results in net thaw → End frost season 12.02.19

Total frost index (FI) for the winter of 2018 - 2019 is hence:

$$FI = 1502.4 - 1173.6 + 4022.4 = 4351.2\ h°C$$

Appendix 7 – Mineral content in rock materials at Jaktøyen field test

The materials used in the superstructure are from three different locations in Trondheim:

Vassfjell

- Crushed rock 22/120 mm
- Crushed rock 0/300 mm

Sjøla

- Crushed rock 0/32 mm
- Crushed rock 0/16 mm
- Crushed rock 22/250 mm

Furuhaugen

- Unsorted gravel

All the following information of rock type content and mineral content are sent per email from Arnhild Ulvik (NPRA), origin from the NGU database for crushed rock and gravel.

Furuhaugen

It is not found any analysis of the gravel from Furuhaugen gravel extraction. However, a report from a neighbor gravel extraction is available, and it is assumed that they are comparable regarding ice movement, water transport, and location relative to Vassfjellet.

Values for thermal conductivity is taken from Cermak and Rybach, 1982, and specific heat from Duba et al, 1990.

Table 3 Rock type content and the appurtenant thermal properties for the gravel from Furuhaugen

Rock type	Content	Thermal conductivity [W/mK]	Specific heat [J/(kg·K)]
Granite Gneiss	28 %	3,14	790
Quartzite	20 %	6,24	770
Greenstone	25 %	2,92	620[1]
Gabbro	5%	2,32	810
Mica Schist	22 %	2,92	650[2]
[1]Mean value from calculations of specific heat of greenstone from Sjøla. [2] Assumed to be 650 J/kgK after values for similar rocks.			

Remark that the analysis of rock type content is executed on 150-250 grains between 8-16 mm and that the grading curve for the specific unsorted gravel shows grains from 0-63 mm. The mineral composition can vary between more fine and coarse grains.

The calculated specific conductivity of particles, k_s, is

$$k_s = (k_n{}^{x_n}) = k_1{}^{x_1} \cdot k_2{}^{x_2} \cdot \ldots = 3.43 \text{ W/mK}$$

And the specific heat for particles, $C_{p,s}$ is

$$C_{p,s} = (x_n C_n) = x_1 C_1 + x_2 C_2 + \cdots = 714 \text{ J/kgK}$$

Sjøla (Greenstone)

All values for thermal conductivity and specific heat are taken from Cermak and Rybach (1982), except the specific heat for epidote which is taken from Duba et al.(1990).

Table 4 Mineral content and the appurtenant thermal properties for rock material from Sjøla

Mineral	Content [%]	Thermal conductivity [W/mK]	Specific heat [J/(kg·K)]
Hornblende	49	2.85	740
Plagioclase	20	1.53-2.31	700
Other minerals	12	3[1]	700[2]
Oxide	5	2.52, 5.12, 11.3	600-700
Sulfide	5	2.28, 8.19, 12.7, 19.2	200-500
Quartz	3	7.69	698
Epidote	3	2.82	720
Calcite	3	3.57	793
[1]A mean value of 3W/mK is assigned to the unknown minerals [2]A mean value of 700 J/kgK is assigned to the unknown minerals			

Specific heat for crushed rock from Sjøla is hence around 700 J/(kg·K) and thermal conductivity for particles is about 3.36 W/mK.

Vassfjell (Gabbro)

Same sources and assumptions as for Sjøla.

Table 5 Mineral content and the appurtenant thermal properties for rock material from Vassfjell

Mineral	Content [%]	Thermal conductivity [W/mK]	Specific heat [J/(kg*K)]
Hornblende	64	2.85	740
Epidote	20	2.82	720
Plagioclase	10	1.53-2.31	700
Serpentine	3	2.34-5.3	720[1]
Calcite	2	3.57	793
Other minerals	1	3[2]	740[3]
[1]Assumed to be 720 J/kgK after values for similar minerals [2]A mean value of 3W/mK is assigned to the unknown minerals [3]A mean value of 740 J/kgK is assigned to the unknown minerals			

For Vassfjell the specific heat is around 730 J/(kg·K) and specific thermal conductivity around 2.85 W/mK.

Appendix 8 – Grain size distribution curves and declaration of performance

Unsorted gravel (F1)
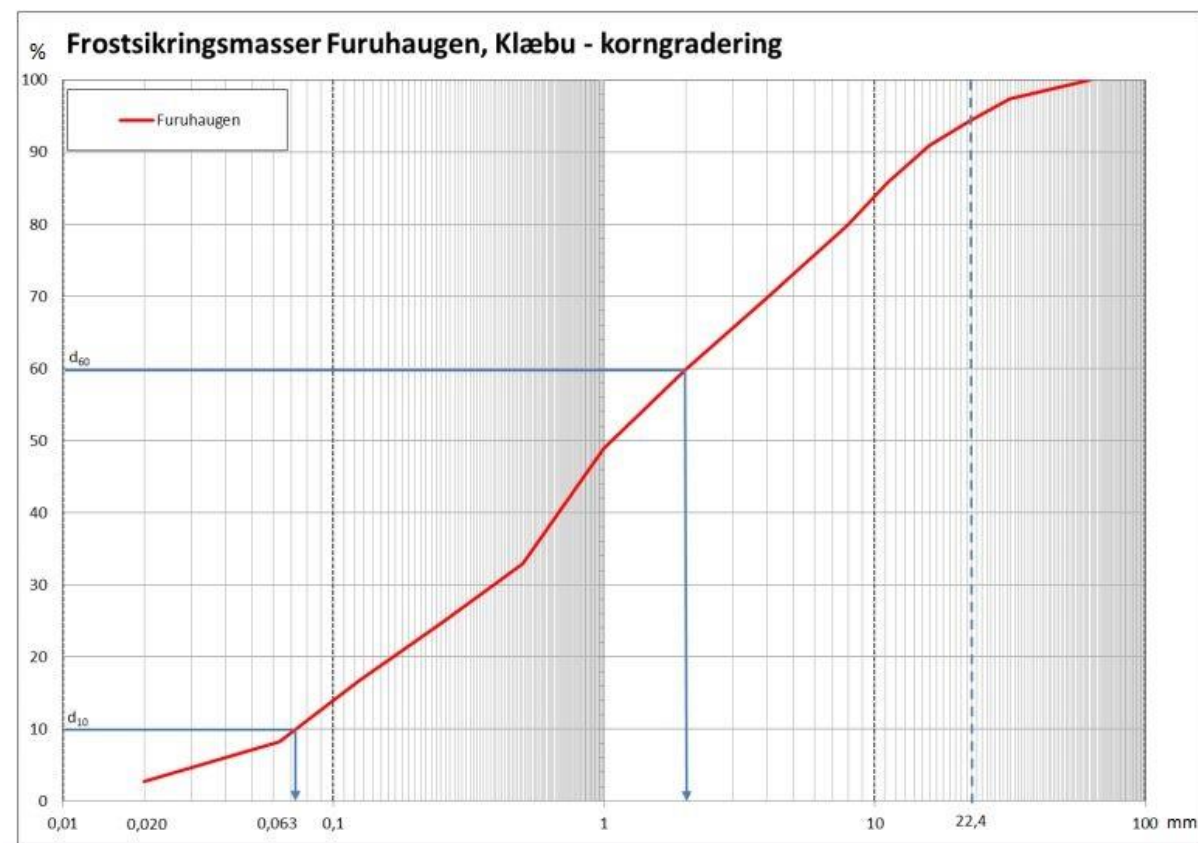
Figure 6 Grain size distribution curve for unsorted gravel

Share of material < 0.020 mm ≈ 3%, share of material < 0.063 = 8.7%, humus content = 1.7 %.

Protective layer and levelling coarse 0/22 (F2)

Table 6 Grain size distribution for crushed rock 0/22

Pr.nr.	µm				mm							
	63	125	250	500	1	2	4	8	11.2	16	22.4	31.5
177(P)	7.4	8.4	9.7	12.1	15.5	21.8	30.1	46.4	59.5	82.2	96.6	100.0
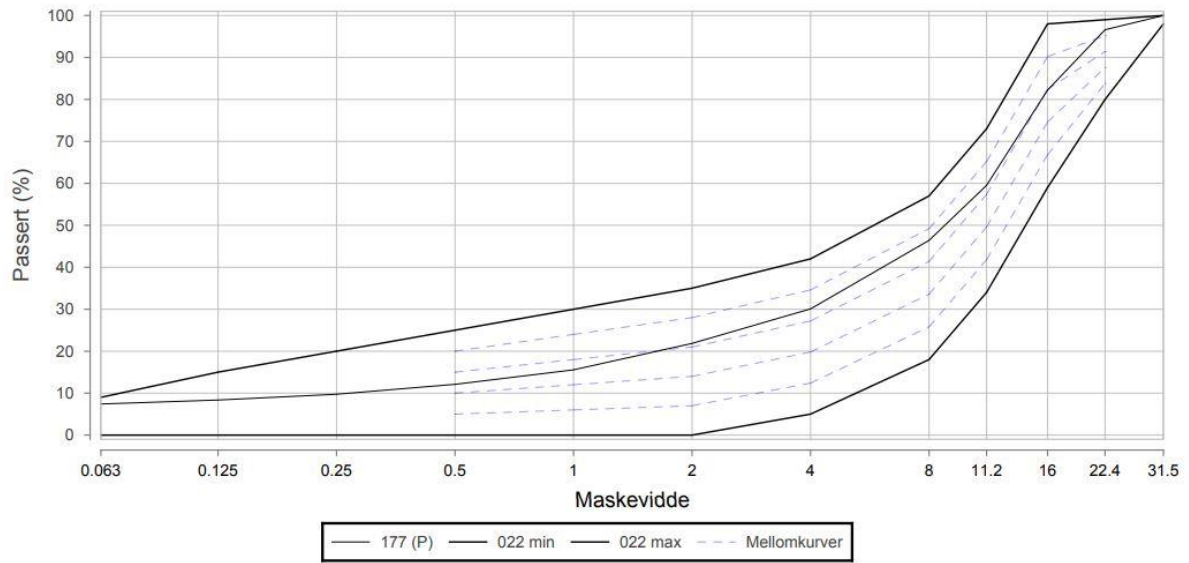
Figure 7 Grain size distribution curve for crushed rock 0/22

0/300 (F2, F3, F4 and F6)

Table 7 Grain size distribution for crushed rock 0/300

Pr.nr.	µm				mm											
	63	125	250	500	1	2	4	8	11,2	16	22.4	31.5	45	63	90	380
For-deling	1.7	2.0	2.7	4.1	5.5	7.5	10.9	17.7	22.5	29.3	36.8	45.7	55.3	62.1	68.2	100
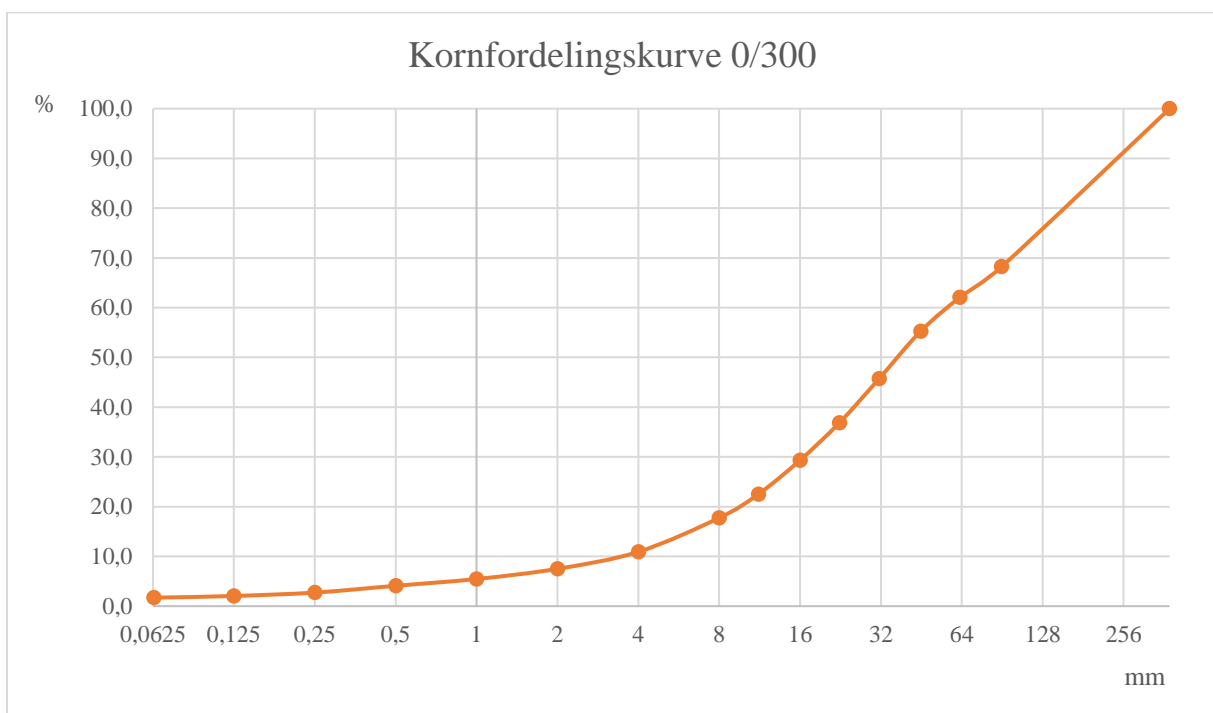
Figure 8 Grain size distribution curve for crushed rock 0/300

0/32 (F5)

Table 8 Grain size distribution for crushed rock 0/32

Pr.nr.	μm				mm							
	63	125	250	500	1	2	4	8	16	22.4	31.5	45
169(P)	3.0	3.5	4.2	4.8	5.4	6.5	8.4	15.2	47.2	72.1	95.3	100.0
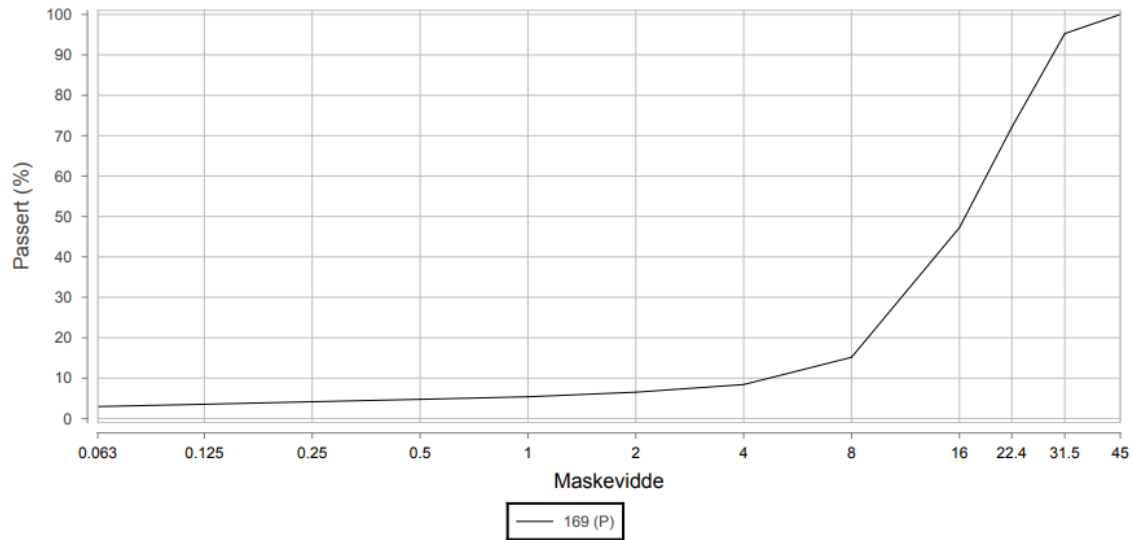
Figure 9 Grain size distribution curve for crushed rock 0/32

22/250 (F7)

Table 9 Grain size distribution for crushed rock 22/250

Pr.nr.	μm				mm								
	63	125	250	500	1	2	4	8	11.2	16	22.4	125	250
282(P)	0.2	0.3	0.3	0.4	0.5	0.7	1.1	2.8	5.0	10.6	13.7	51.5	96.0
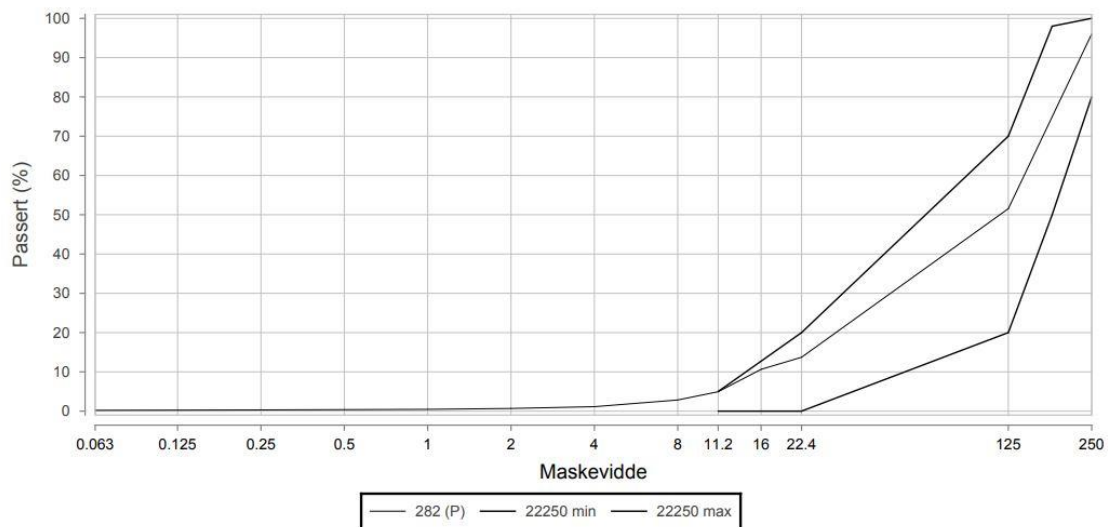
Figure 10 Grain size distribution curve for crushed rock 22/250

Foam glass 10/60 (F4)

The technical material parameters are taken from producer (Glasopor, u.d.).

Materialtekniske parametere for Glasopor® skumglass 10–60

Lette fyllinger/frostisolasjon	Testmetode	Størrelse
Kornstørrelse	NS-EN 933-1	10–60 mm
Tørr densitet (løs bulkdensitet)	NS-EN 1097-3	180 kg/m³
Korndensitet, prd	NS-EN 1097-6	380 kg/m³
Motstand mot knusing (ved 20% kompresjon)	NS-EN 13055	0,77 MPa
Bæreevnegruppe ved dimensjonering av overbygning		4*
Dimensjonerende tyngdetetthet i fylling	NS-EN 1097-3	3,0 kN/m³*
Dimensjonerende tyngdetetthet mot oppflyting	NS-EN 1097-3	2,2 kN/m³
Kapillær stigehøyde	NS-EN 1097-10	170 mm
Volumendring ved komprimering	NS-EN 1097-10	15–25 %
Friksjonsvinkel		45 °
Varmekonduktivitet (tørr)	NS-EN 12667	0,097 W/mK
Varmekonduktivitet (våt-drenert)	NS-EN 12667	0,107 W/mK
Fryse-/tinemotstand	NS-EN 13055-2	0,2 %
Utlegging – maksimal lagtykkelse		Inntil landkar /støttemur: 0,6 m Lettfylling: 1,0 m Grøfter: 0,3 m
Komprimering		Beltegående maskin med beltetrykk < 50 kN/m² Vibroplate ved landkar/ støttemur 50–200 kg

Figure 11 Technical material parameters for Foam glass 10-60mm

Lightweight aggregate 0/32 (F6)

Declaration of performance for LECA taken from producer (Leca, 2014).

Vesentlige egenskaper Essential characteristics	Ytelse Performance	
Brannpåvirkning Reaction to fire	Euroclass A1 (according Commission Decision 2000/605/EC)	
Vannpermeabilitet Water permeability	$> 10^{-3}$ m/s	
Utlekking av kjemiske stoffer Release of dangerous substances	NPD	
Varmemotstand Thermal resistance	Thermal conductivity	< 0,12 W/mK
	Loose bulk density	275 kg/m³ ±15%
	Aggregate size	0-32 mm
Vanndamptransmisjon Water vapour transmission	2	
Trykkfasthet Compressive strength	CS (10): > 1300 kPa CS (2) : > 500 kPa	
Motstand mot dynamisk last Resistance to dynamic loads	< 1,0 % (120 kPa, 2 000 000 cycles)	
Endringer i brannmotstand ved aldring/degradering Durability of reaction to fire against ageing/degradation	Endres ikke over tid	
Endringer i varmemotstand ved aldring/degradering Durability of thermal resistance against ageing/degradation	Endres ikke over tid	
Endringer i trykkfasthet ved aldring/degradering Durability of compressive strength against ageing/degradation	Endres ikke over tid	
Endringer i dynamisk last ved aldring/degradering Durability of resistance to dynamic loads against ageing/degradation	Endres ikke over tid	
Endringer i motstand mot kjemisk og biologisk angrep ved aldring/degradering Durability against chemicals and biological attack	Endres ikke over tid	

NPD = ingen angitt ytelse / No Performance Determined

8.   Bruk av hensiktsmessig teknisk dokumentasjon og/eller spesifikk teknisk dokumentasjon
Appropriate Technical Documentation and/or Specific Technical Documentation: Ikke relevant/Not applicable

Ytelser for denne byggevaren som er anført ovenfor, er i overensstemmelse med de angitte ytelsene. Denne ytelseserklæringen er utarbeidet i overensstemmelse med forordning (EU) nr. 305/2011 under produsentens eneansvar, som anført ovenfor. / The performance of the product identified above is in conformity with the set of declared performance/s. This declaration of performance is issued, in accordance with Regulation (EU) No 305/2011, under the sole responsibility of the manufacturer identified above.

Underskrevet for produsenten og på dennes vegne av /
Signed for and on behalf of the manufacturer by:

....Ian Tange..
(Navn / name)

cAt Leca Rælingen, Norway...............   ......25. november 2016.......
(Sted / place)   (Dato / date of issue)

....
(signature)

Figure 12 Declaration of performance for LECA lightweight aggregate

XPS 500 (F2)

Declaration of performance for XPS is taken from producer (Sundolitt, 2018).

Sundolitt

Declaration of Performance
NO-21110-CPR

1 Product-type	Boards of extruded polystyrene (XPS)
2 Identification	Sundolitt® XPS. Product name, product specification, identification and production date is marked on the product, on the packaging, or on the label put on the packaging.
3 Intended use	Sundolitt® XPS is intended as a load-bearing thermal insulation for construction and civil engineering applications.

4 Name and contact address of the manufacturer

Brødr. Sunde as, PO Box 8115 Spjelkavik, N-6022 Ålesund. Ph.: 70 17 70 00.

5 System of assessment and verification of constancy of performance (AVCP)

System 3 according to EN 13164:2012+A1:2015

6 Notified body and tasks performed Teknologisk Institutt (ID-number 1235) has performed ITT-testing according to System 3.

7 Declared performance according to EN 13164:2012.

8 Declared performance

	XPS250	XPS300	XPS400	XPS500	XPS700
Thickness	T1	T1	T1	T1	T1
Reaction to fire	Euroclass F	Euroclass F	Euroclass F	Euroclass F	Euroclass F
Compressive stress	CS(10\Y)250	CS(10\Y)300	CS(10\Y)400	CS(10\Y)500	CS(10\Y)700
Dimentional stability	Class DS(23,90)	Class DS(23,90)	Class DS(23,90)	Class DS(23,90)	Class DS(23,90)
Water absorpt.long.term by imm.	WL(T)0,7	WL(T)0,7	WL(T)0,7	WL(T)0,7	WL(T)0,7
Water absorpt.long.term by dif.	WD(V)2	WD(V)2	WD(V)2	WD(V)2	WD(V)2
Water absorpt.long.term by fr/th	FTCD1	FTCD1	FTCD1	FTCD1	FTCD1

Insulation properties Sundolitt XPS 250-700											
Thickness	d_N [mm]	30	40	50	60	70	75	80	100	120	150
Sundolitt XPS 250	λ_D [W/(mK)]	0,033			0,034				0,036	0,039	
Sundolitt XPS 300	λ_D [W/(mK)]	0,033			0,034				0,036	0,039	
Sundolitt XPS 400	λ_D [W/(mK)]	0,034							0,036	0,039	
Sundolitt XPS 500	λ_D [W/(mK)]	0,034							0,036	0,039	
Sundolitt XPS 700	λ_D [W/(mK)]	0,034							0,036	0,039	

The performance of Sundolitt® XPS is in compliance with the declared values. This DoP is issued in compliance with the regulation (EU) 305/2011.

Signed on behalf of Brødr. Sunde as by:

Karl Martin Sagstuen
Skedsmo, August 17. 2018

Brødr. Sunde as
6022 Ålesund · Norge · Tlf.: + 47 70 17 70 00
www.sundolitt.no · norway@sundolitt.com
Org.nr 916 416 784

Figure 13 Declaration of performance for XPS

Appendix 9 – Results from numerical analysis

	Sensor	Depth	Ref. data	Mod. res.	ΔT	Sensor	Depth	Ref. data	Mod. res.	ΔT
			06.02.2019					**13.03.2019**		
F1	8	0	-10,3	-10,4	0,11	8	0	1,5	-0,7	2,24
	7	-0,225	-10,4	-9,7	0,73	7	-0,225	-1,9	-1,4	0,45
	6	-0,6	-5,6	-5,45	0,19	6	-0,6	-0,7	-1,1	0,36
	5	-1,025	-2,3	-1,85	0,44	5	-1,025	0,4	0,034	0,37
	4	-1,55	-1,7	-0,2	1,46	4	-1,55	1,0	1,2	0,21
	3	-2,125	-0,8	1,1	1,86	3	-2,125	1,6	2,04	0,41
	2	-2,35	-0,3	1,7	1,96	2	-2,35	2,1	2,4	0,33
	1	-2,575	0,2	2,3	2,07	1	-2,575	2,6	2,75	0,20
	-1	-3,13	1,7	3,75	2,08	-1	-3,13	4,1	3,6	0,52
	-2	-4,13	6,07	6,07	0,00	-2	-4,13	5,1	5,1	0,05
F2	12	0	-9,9	-10,4	0,47	12	0	1,9	-0,7	2,58
	11	-0,225	-11,3	-9,75	1,51	11	-0,225	-52004,0	-1,42	0,12
	10	-0,6	-6,5	-6,78	0,28	10	-0,6	-1,5	-1,14	0,38
	9	-1,025	-3,0	-4,23	1,26	9	-1,025	-0,5	0,13	0,65
	8	-1,15	-2,4	-3,96	1,59	8	-1,15	0,2	0,3	0,06
	7	-1,3	-2,1	-3,7	1,60	7	-1,3	0,4	0,48	0,06
	6	-1,35	0,2	0,35	0,11	6	-1,35	2,8	2,95	0,14
	5	-1,475	0,4	-0,17	0,60	5	-1,475	3,0	3,1	0,15
	4	-1,775	0,9	0,4	0,52	4	-1,775	3,5	3,483	0,03
	3	-2,125	1,3	1,07	0,25	3	-2,125	4,0	3,88	0,13
	2	-2,35	1,5	1,5	0,01	2	-2,35	4,1	4,1	0,02
	1	-2,575	5,3	x	x	1	-2,575	4,3	x	x
F3	8	0	-10,3	-10,4	0,15	8	0	2,08	-0,7	2,78
	7	-0,225	-11,5	-9,52	2,01	7	-0,225	-1,32	-1,4	0,08
	6	-0,6	-7,6	-6,25	1,39	6	-0,6	-1,04	-1,1	0,06
	5	-1,025	-3,3	-3,25	0,02	5	-1,025	0,97	0,36	0,61
	4	-1,55	-1,5	-1,64	0,18	4	-1,55	1,91	1,452	0,46
	3	-2,125	-0,2	-0,33	0,15	3	-2,125	2,63	2,45	0,18
	2	-2,35	0,2	0,2	0,03	2	-2,35	2,75	2,75	0,00
	1	-2,575	4,0	x	x	1	-2,575	2,99	x	x

Figure 14 Results for F1, F2, and F3

	06.02.2019				13.03.2019			
	Sensor	Depth	Ref. data	Mod. res.	ΔT	Sensor	Depth	Ref. data	Mod. res.	ΔT
F4	10	0	-10,6	-10,4	0,16	10	0	2,2	-0,7	2,87
	9	-0,225	-11,9	-9,8	2,06	9	-0,225	-1,3	-1,44	0,16
	8	-0,6	-8,4	-7,2	1,16	8	-0,6	-1,4	-1,25	0,17
	7	-1,025	-4,7	-4,88	0,23	7	-1,025	0,3	0,02	0,31
	6	-1,15	-2,7	-2,14	0,61	6	-1,15	1,5	1,7	0,25
	5	-1,325	0,8	0,75	0,08	5	-1,325	3,7	3,65	0,04
	4	-1,7	1,6	1,2	0,37	4	-1,7	4,3	4,02	0,24
	3	-2,125	1,8	1,7	0,07	3	-2,125	4,4	4,4	0,02
	2	-2,35	2,1	1,95	0,11	2	-2,35	4,6	4,6	0,00
	1	-2,575	2,2	2,2	0,01	1	-2,575	4,8	4,8	0,01
F5	8	0	-49134,00	-10,4	0,1	8	0	-52041,0	-0,7	2,7
	7	-0,225	-11,43	-9,45	1,98	7	-0,225	-1,3	-1,4	0,06
	6	-0,6	-6,64	-6	0,64	6	-0,6	-0,9	-1,06	0,19
	5	-1,025	-2,74	-2,77	0,03	5	-1,025	0,6	0,39	0,21
	4	-1,55	-1,43	-1,54	0,11	4	-1,55	1,5	1,17	0,36
	3	-2,125	-0,60	-0,52	0,08	3	-2,125	2,1	1,92	0,17
	2	-2,35	-0,15	-0,15	0,00	2	-2,35	2,3	2,3	0,00
	1	-2,575	3,27	x	x	1	-2,575	2,6	x	x
F6	10	0	-10,2	-10,4	0,17	10	0	1,7	-0,7	2,45
	9	-0,225	-11,5	-9,75	1,73	9	-0,225	-1,2	-1,44	0,19
	8	-0,6	-8,5	-7,08	1,43	8	-0,6	-1,2	-1,23	0,02
	7	-1,025	-5,5	-4,74	0,78	7	-1,025	0,5	0,23	0,25
	6	-1,15	-2,9	-2,52	0,41	6	-1,15	1,7	1,7	0,01
	5	-1,325	0,1	0,02	0,09	5	-1,325	3,2	3,47	0,24
	4	-1,7	0,9	0,65	0,21	4	-1,7	3,7	3,91	0,17
	3	-2,125	1,5	1,46	0,08	3	-2,125	4,3	4,32	0,03
	2	-2,35	1,9	1,9	0,02	2	-2,35	4,5	4,5	0,02
	1	-2,575	5,7	x	x	1	-2,575	4,8	x	x
F7	8	0	-11,0	-10,4	0,57	8	0	1,0	-0,75	1,79
	7	-0,225	-10,1	-9,6	0,52	7	-0,225	-1,8	-1,45	0,33
	6	-0,6	-5,9	-6,48	0,55	6	-0,6	-0,4	-1,25	0,89
	5	-1,025	-3,2	-3,7	0,46	5	-1,025	0,3	0,06	0,21
	4	-1,55	-2,5	-1,74	0,73	4	-1,55	1,1	1,25	0,12
	3	-2,125	-1,3	0	1,26	3	-2,125	2,4	2,36	0,06
	2	-2,35	-0,8	0,58	1,34	2	-2,35	2,7	2,65	0,05
	1	-2,575	-0,3	1,22	1,47	1	-2,575	3,0	2,94	0,08
	-1	-3,13	1,3	2,87	1,58	-1	-3,13	4,0	3,7	0,33
	-2	-4,13	6,0	6	0,03	-2	-4,13	5,1	5,1	0,00

Figure 15 Results for F4, F5, F6, and F7

Depth [m]	Average variation of 06.02 and 13.03						
	F1	F2	F3	F4	F5	F6	F7
0	1,2	1,5	1,5	1,5	1,4	1,3	1,2
-0,225	0,6	0,8	1,0	1,1	1,0	1,0	0,4
-0,6	0,3	0,3	0,7	0,7	0,4	0,7	0,7
-1,025	0,4	0,9	0,3	0,3	0,1	0,5	0,3
-1,15		0,8		0,4		0,2	
-1,3		0,8					
-1,325				0,1		0,2	
-1,35		0,4					
-1,475		0,4					
-1,55	0,8		0,3		0,2		0,4
-1,7				0,3		0,2	
-1,775		0,3					
-2,125	1,1	0,2	0,2	0,0	0,1	0,1	0,7
-2,35	1,1	0,0	0,0	0,1	0,0	0,0	0,7
-2,575	1,1			0,0			0,8
-3,13	1,3						1,0
-4,13	0,0						0,0
Average for all depths	0,79	0,58	0,57	0,45	0,46	0,47	0,62
Mean average:				0,56			

Figure 16 Average variation between modeled results and reference data

References

Cermak, V. & Rybach, L., 1982. *Thermal properties: Thermal conductivity and specific heat of minerals and rocks,* s.l.: s.n.

Côté, J. K. J.-M., 2004. *A generalized thermal conductivity model for soils and construction materials,* Québec: s.n.

Duba, A. G., Durham, W. B., Handin, J. W. & Wang, H. F., 1990. *The Brittle-Ductile Transition in Rocks: The Heard Volume.* s.l.:s.n.

Glasopor, u.d. *Teknisk brosjyre, Glasopor skumglass 10-60.* [Internett]
Available at: https://www.glasopor.no/dokumentasjon/tekniske-spesifikasjoner/
[Funnet 29 Mars 2019].

Leca, 2014. *Leca lettklinker 0-32 mm.* [Internett]
Available at: https://leca.no/produkter/leca-kuler/leca-lettklinker-0-32-mm/
[Funnet 17 05 2019].

Sundolitt, 2018. *Ytelseserklæringer - Sundolitt XPS.* [Internett]
Available at: http://www.sundolitt.no/sundolitt/dokumentasjon/ytelseserklaringer/sundolitt-xps
[Funnet 29 05 2019].